(2)

NAVAL POSTGRADUATE SCHOOL

Monterey, California

THESIS

TRANSVERSE VIBRATIONS OF A COMPOSITE CYLINDRICAL TUBE OF CIRCULAR CROSS SECTION

by

Raymond William Etter

September, 1989

Thesis Advisor: Michael R. Gorman

Unclassified
SECURITY CLASSIFICATION OF THIS PAGE

REPORT DOCUMENTATION PAGE

Form Approved OMB No. 0704-0188

1a. REPORT SECURITY CLASSIFICATION UNCLASSIFIED	1b. RESTRICTIVE MARKINGS
2a. SECURITY CLASSIFICATION AUTHORITY Multiple Sources	3 DISTRIBUTION / AVAILABILITY OF REPORT Approved for public release; distribution is unlimited
2b. DECLASSIFICATION / DOWNGRADING SCHEDULE	
4. PERFORMING ORGANIZATION REPORT NUMBER(S)	5. MONITORING ORGANIZATION REPORT NUMBER(S)
6a. NAME OF PERFORMING ORGANIZATION Naval Postgraduate School 6b. OFFICE SYMBOL (If applicable) 39	7a. NAME OF MONITORING ORGANIZATION Naval Postgraduate School
6c. ADDRESS (City, State, and ZIP Code) Monterey, CA 93940-5000	7b. ADDRESS (City, State, and ZIP Code) Monterey, CA 93940-5000
8a. NAME OF FUNDING / SPONSORING ORGANIZATION 8b. OFFICE SYMBOL (If applicable)	9 PROCUREMENT INSTRUMENT IDENTIFICATION NUMBER
8c. ADDRESS (City, State, and ZIP Code)	10. SOURCE OF FUNDING NUMBERS PROGRAM ELEMENT NO. / PROJECT NO. / TASK NO / WORK UNIT ACCESSION NO.

11. TITLE (Include Security Classification)
TRANSVERSE VIBRATIONS OF A COMPOSITE TUBE OF CIRCULAR CROSS SECTION

12. PERSONAL AUTHOR(S)
Etter, Raymond, W.

13a. TYPE OF REPORT Master's Thesis	13b. TIME COVERED FROM _____ TO _____	14. DATE OF REPORT (Year, Month, Day) September, 1989	15. PAGE COUNT 115

16. SUPPLEMENTARY NOTATION
The views expressed in this thesis are those of the author and do not reflect the official policy or position of the Department of Defense or the U.S. Government

17. COSATI CODES		
FIELD	GROUP	SUB-GROUP

18. SUBJECT TERMS (Continue on reverse if necessary and identify by block number)
composite, shell, laminate, modal analysis, vibration tube, Euler-Bernoulli, laminated plate, laminated shell

19. ABSTRACT (Continue on reverse if necessary and identify by block number)
The transverse frequencies of vibration of laminated orthotropic cylindrical shells were studied in order to compare experimental results with results predicted by a modified Euler-Bernoulli beam theory. The structures studied had circular cross sections and were made of graphite/epoxy. Stacking sequences for the test structures were [90,±60$_3$,90] and [90,±45$_3$,90]. The structures were tested under clamped-free boundary conditions. Testing was conducted by measuring the Frequency Response Function (FRF) of the structure after exciting it with a modal hammer. Response was measured using an accelerometer. Signal processing was done with a digital signal analyzer and FRFs were analyzed using modal analysis software. The experimental data were used to derive a modal model of the test structure. Analytical predictions were made by one dimensionalizing the two dimensional laminated plate theory equations of motion. Treatment of the test structures as a beam was justified by investigating the equations of motion of classical shell theory and making physically reasonable assumptions,

20. DISTRIBUTION / AVAILABILITY OF ABSTRACT ☐ UNCLASSIFIED/UNLIMITED ☐ SAME AS RPT ☐ DTIC USERS	21. ABSTRACT SECURITY CLASSIFICATION Unclassified
22a. NAME OF RESPONSIBLE INDIVIDUAL Michael Gorman	22b TELEPHONE (Include Area Code) 408- 646-2074 22c. OFFICE SYMBOL 67 Go

DD Form 1473, JUN 86 Previous editions are obsolete. S/N 0102-LF-014-6603

SECURITY CLASSIFICATION OF THIS PAGE
Unclassified

Approved for public release; distribution is inlimited

Transverse Vibrations of a Composite Cylindrical Tube of Circular Cross Section

by

Raymond William Etter
Captain, United States Marine Corps
B.S.,Rensselaer Polytechnic Institute, 1983

Submitted in partial fulfillment of the
requirements for the degree of

MASTER OF SCIENCE IN AERONAUTICAL ENGINEERING

from the

NAVAL POSTGRADUATE SCHOOOL
September, 1989

Author: Raymond William Etter
Raymond William Etter

Approved By: Michael R. Gorman
Michael R. Gorman, Thesis Advisor

Edward M. Wu, Second Reader

E. R. Wood
Edward R. Wood , Chairman, Department of Aeronautics and Astronautics

Approved for public release; distribution is unlimited

Transverse Vibrations of a Composite Cylindrical Tube of Circular Cross Section

by

Raymond William Etter
Captain, United States Marine Corps
B.S.,Rensselaer Polytechnic Institute, 1983

Submitted in partial fulfillment of the
requirements for the degree of

MASTER OF SCIENCE IN SYSTEMS TECHNOLOGY
(SPACE SYSTEMS OPERATIONS)

from the

NAVAL POSTGRADUATE SCHOOOL
September, 1989

Author: Raymond W. Etter
Raymond William Etter

Approved By: Michael R. Gorman
Michael R. Gorman, Thesis Advisor

Edward M. Wu
Edward M. Wu, Second Reader

Rudolph Panholzer
Rudolph Panholzer, Chairman, Space Systems Academic Group

ABSTRACT

The transverse frequencies of vibration of laminated orthotropic cylindrical shells were studied in order to compare experimental results with results predicted by a modified Euler-Bernoulli beam theory. The structures studied had circular cross sections and were made of graphite/epoxy. Stacking sequence for the test structures were $[90,\mp 60_3,90]$ and $[90,\mp 45_3,90]$. The structures were tested under clamped-free boundary conditions. Testing was conducted by measuring the Frequency Response Function (FRF) of the structure after exciting it with an impulse from a modal hammer. Response was measured using an accelerometer. Signal processing was done with a digital signal analyzer and FRFs were analyzed using modal analysis software. The experimental data were used to derive a modal model of the test structure.

Analytical predictions were made by one dimensionalizing the two dimensional laminated plate theory equations of motion. Treatment of the test structures as a beam was justified by investigating the equations of motion of classical shell theory and making physically reasonable assumptions.

TABLE OF CONTENTS

LIST OF SYMBOLS

A	Inertance frequency response function for single degree of freedom discrete system
$_rA_{ij}$	Modal constant
A,B,D	Stiffness matrices
b	Width
c	Damping coefficient
c_{crit}	Critical damping coefficient
C_{ijkl}	Stiffness tensor
C_{ij}	Stiffness matrix
C	Damping matrix for multi degree of freedom systems
d	Depth
$\mathbf{d}^*$	Inverse of the bending stiffness matrix
E	Young's modulus
E[]	Expected value of
f	Force
f_n	Natural frequency in hertz
$_rf_d$	Damped natural frequency of the r^{th} mode
FRF	Frequency response function
F'	Force impulse
FT	Fourier transform
$F(\omega)$	Fourier transform of the force
$\mathcal{F}\{\}$	Fourier transform of
h	Wall thickness
$H(\omega)$	Transfer function

Hz	Hertz, cycles per second
I	Area moment of inertia
Im{}	Imaginary part of
k	Spring constant
$\mathbf{K}$	Stiffness matrix for multi degree of freedom systems
$\mathbf{K}_r$	Diagonalized generalized stiffness matrix
l	Length
m	Mass
m	Mass per unit length
MDOF	Multi degree of freedom
$\mathbf{M}$	Mass matrix for multi degree of freedom systems
$\mathbf{M}$	Column vector of moment resultants
$\mathbf{M}_r$	Diagonalized generalized mass matrix
$\mathbf{N}$	Column vector of stress resultants
Q	Quality factor
$\mathbf{Q}$	Reduced stiffness matrix
R	Radius of curvature of the midplane
Re{}	Real part of
S_{ijkl}	Compiance tensor
S_{ij}	Compliance matrix
SDOF	Single degree of freedom
TF	Transfer function
u,v,w	Displacements
$\mathbf{u}$	Column vector of displacement magnitudes
$X(\omega)$	Fourier transform of the displacement

Y	Mobility frequency response function for single degree of freedom discrete system
$\alpha(\omega)$	Receptance frequency response function for single degree of freedom discrete system
$\alpha_{ij}(\omega)$	Receptance matrix for multi degree of freedom systems
β_n	Mode factor
γ	Column vector of force magnitudes
δ	Dirac delta function
ϵ	Column vector of the strains
ϵ_{ij}	Strain tensor
ϵ_i	Contracted strain
ϵ_x	Normal strain in the x direction
ϵ_s	Normal strain in the s direction
ϵ_{xs}	In plane shearing strain
ζ	Damping factor (= c/c_{crit})
κ	Column vector of the curvatures
ρ_o	Mass density per unit volume
σ_{ij}	Stress tensor
σ_i	Contracted stress
$\phi(\omega)$	Phase angle
Φ_r	Normalized eigenvector associated with the r^{th} mode of vibration
${}_r\Phi_i$	r^{th} element of the i^{th} normalized eigenvector
Φ	Normalized modal matrix
ψ_r	Eigenvector associated with the r^{th} mode of vibration
${}_r\psi_i$	r^{th} element of the i^{th} eigenvector
Ψ	Modal matrix
ω	Circular frequency

ω_n	Natural frequency
ω_d	Frequency of damped vibration
ω_r	Resonant frequency
Ω_r^2	Diagonalized matrix with the diagonal elements equal to the natural frequencies
$\mathbf{1}$	Diagonalized identity matrix

ACKNOWLEDGEMENTS

This author sincerely thanks Professor Michael Gorman for his guidance, patience, and encouragement throughout the course of his graduate studies and through the completion of this thesis. Appreciation is extended to the author's second reader, Professor Edward Wu, for providing his wisdom and insight to the author's graduate education. A special thank you to Mr. James L. Koury of the Air Force Astronautics Laboratory for his encouragement and support of this work. The author would like to acknowledge the efforts of the staff of the Composite Materials Lab at the Air Force Astronautics Laboratory for kindly providing the composite tube specimens used in this work. The author would also like to thank the Naval Postgraduate School Research Council and Dr William Scott of the Naval Air Development Center for their partial support of this work. Not enough thanks can go to Steve Ziola for his patience and help in the lab. This work is dedicated to my family. Without their support this opportunity could never have occurred.

I. INTRODUCTION

With the advent of large flexible space structures renewed interest in the vibration of shell structures has come about . The governing equations of shell structures are quite complex. What is required by the practicing engineer are equations which are both easy to use and give a good representation of the system being designed. Of interest in this work was determing experimentally if a homogeneous anisotropic cylinder with a circular cross section could be modelled analytically as an Euler-Bernoulli beam. The desired results were an equation in simplified form which would predict the natural frequencies of transverse vibration.

A detailed computer aided literature search through the Defense Technical Information Services, Defense Technical Information Center, and the National Aeronautics and Space Administration lists of references revealed 75 papers relating to the topic of this work. Further investigation of these papers reduced the number to twelve papers. Ten of the twelve papers presented analytical results and the remaining two presented experimental results. However, the two papers which presented the experimental results were for work done on isotropic materials. A brief description will be given of the papers described above. It will be seen that a simplified analytical treatment of shells did not appear in the literature.

Dong, Pister, and Taylor [Ref. 1] presented a small deflection theory to formulate the equations of motion for laminated anisotropic shells and plates. In this paper a generalized set of equations is derived which result in eighth order partial differential equations. In a paper by Dong [Ref. 2] the free vibration of laminated orthotropic cylindrical shells are treated. In this paper Dong presents an

iterative method which will result in the natural frequencies of the shell. In this method the solution requires solving for the eigenvalues for an eighth order system. A more recent work by Dong and Selna [Ref. 3] presents a finite element approach to the free vibration of shells. This method requires a minimal amount of computer of time, but does not provide the physical intuitiveness we are seeking.

In a work by Das [Ref. 4] the equation of motion of orthotropic cylindricl shells again requires the solution of an eighth order partial differential equation. This paper does not account for arbitrary orientations of layered material. In another work by Das and Rath [Ref. 5] the vibration of layered shells is considered. In this work the effect of shear deformation is included. This paper again presents lengthy higher order differential equations. Papers by Soedel [Ref. 6], Loewy and Stavsky [Ref. 7], Baker, Bert, and Egle [Ref. 8] present work much along the same lines as those mentioned above. In short, none of the papers investigated presented an analysis of shell structures for "back of the envelope calcualtions". Most recently, work done by Darvizeh and Sharma [Ref. 9] present a new approach to the determination of the natural frequencies of laminated orthotropic thin circular cylinders. However, these results also do not have the heuristic attributes of "back of the envelope calculations".

Experimental work done by Weingarten [Ref. 10] and Bray and Egle [Ref. 11] give results which correlate well with values predicted by classical shell theory. However, these results are not directly related to the objectives of this work because the results are for isotropic materials. To the extent of the literature searched there exists no published results for the transverse vibrations of composite tubes.

The study of shells is difficult not only because the governing partial differential equations are of eighth order, but there is not agreement among academicians on the correct form of the "classical" shell equations. This perhaps explains the number of papers on the higher order theory and no papers on a simplified model of shell structures. Many shell theories exist and carry the name of the individual who is responsible. Some of these include Donnell, Flügge, Love, Reissner, Timoshenko, and Vlaslov. An excellent reference which summarizes the various shell theories of shell vibration and their results is presented by Leissa [Ref. 12]. For the purposes of this work results given by Donnell will be used to simplify the treatment of shells.

Current research being done at the Air Force Astronautics Laboratory (AFAL) at Edwards Air Force Base, California emphasizes the need for simplified shell equations. The test structures for this work were provided by AFAL. Current research at AFAL includes the vibration characteristics of thin composite shells and control of large flexible structures. The understanding of the vibration characteristics of large flexible structures is critical in order to understand the problems of control. This need for a simplified treatment of shell structures and experimental data to support the analytical results was the motivaton for this work.

II. THEORETICAL BACKGROUND

A. INTRODUCTION

This chapter serves a twofold purpose. First to lay the theoretical groundwork for the measurement techniques used in the experiment and secondly, to provide the background needed to derive the mathematical model of the test structure. For these reasons the sections following this introduction have been titled Experimental and Analytical respectively.

In the Experimental section of this chapter, the equations of motion of discrete mechanical systems will be presented. Both single degree of freedom (SDOF) and multi degree of freedom (MDOF) systems will be considered. The SDOF systems analysis was used to derive the equations of motion of vibration measuring instruments and to understand the uncoupled equations of motion of the MDOF system. We will derive the modal model of the test structure from our understanding of MDOF systems analysis.

In the analytical section of this chapter equations of motion for the flexural vibrations of the structure will be derived. The method used will one dimensionalize the two dimensional laminated plate theory equations of motion. In conclusion, the resulting equation will be shown to give a reasonable prediction with respect to shell theory.

B. DISCRETE SYSTEMS

In vibration analysis we are concerned with determining the mass, damping, and stiffness characteristics (modal parameters) of a structure. From this information we can determine the natural frequencies and mode shapes (also

called modal parameters) of a structure. With this information we can fully describe the dynamic behavior of the structure under any conditons within the assumptions of the the theory. To study these characteristics we must begin by formulating a model which can be applied experimentally. To satisfy this requirement we begin by modelling the system as a discrete mechanical system. A discrete mechanical system is a system in which the mass, damping, and stiffness are lumped into elements. These elements are joined in parallel or series to form the system. An example of a discrete system is a mass attached to a spring and viscous dashpot. Figure 1 is a diagram of such a system. In the discrete system, mass forces are proportional to acceleration ($F = m\ddot{x}$), viscous dashpot forces are proportional to velocity ($F = -c\dot{x}$), and spring forces are proportional to displacement ($F = -kx$). The coefficient m is the mass of the block, c the damping coefficient of the dashpot, and k the stiffness of the spring. The equation(s) of motion for the discrete system are then derived from these relationships and Newton's laws.

The dynamic behavior of discrete systems are described by ordinary differential equations. Discrete systems are defined by the number of degrees of freedom they possess. The degrees of freedom of a system are the number of independent coordinates needed to fully describe the state (motion) of the system. Discrete systems may be single degree of freedom (SDOF) systems (one coordinate required) or multi degree of freedom (MDOF) systems (more than one coordinate required).

Equations of motion for free and forced response of the SDOF and the MDOF systems will be presented. Free response is subjecting the system to a set of initial conditions and observing the resultant motion. A powerful method of analysis,

modal analysis, will be described and used to study the MDOF system. In this work only linear systems were considered.

1. Single Degree of Freedom

The simplest SDOF system to study is the undamped mass-spring system. The undamped mass-spring system is shown in Figure 2. The equation of motion for this system is

$$m\ddot{x} + kx = f.$$

In the absence of an applied force ($f=0$), this reduces to the free response analysis. The new equation of motion is that of the simple harmonic oscillator.

$$m\ddot{x} + kx = 0$$

Using complex notation we can show the solution to be of the form

$$x = Xe^{i\omega_n t},$$

where X is dependent upon the initial conditions and $\omega_n = \sqrt{(k/m)}$, is the natural frequency of the system.

We now let $f \neq 0$ and study the forced response. We will assume f to be harmonic with frequency ω and write f in the following way

$$f = Fe^{i\omega t}.$$

The solution can be shown to have the form

$$x = Xe^{i\omega t}.$$

Substituting the solution into the equation of motion results in the equation

$$(k - \omega^2 m)Xe^{i\omega t} = Fe^{i\omega t}.$$

Cancelling and rearranging terms we arrive at the system receptance frequency response function (FRF).

$$X/F = 1/(k - \omega^2 m) = \alpha(\omega)$$

The receptance FRF is the ratio of harmonic displacement to harmonic excitation. It is interesting to note that the receptance is independent of the forcing function and only a function of the system characteristics (mass and stiffness) and forcing frequency. If we had solved the equation of motion using the Fourier Transform we would have arrived at the result

$$X/F = 1/(k - \omega^2 m) = H(\omega),$$

where $H(\omega)$ is the system transfer function. This equivalence between the FRF and the transfer function is very important in experimentally determining the modal parameters of the system. This relationship allows us to measure the response signal (via electrical signal from transducers) of the measuring instruments and from this relationship derive the mechanical properties of the system.

Other FRF's exist and are related to the receptance. These are the mobility and inertance. The mobility is the ratio of harmonic velocity to harmonic excitation. For sinusoidal excitation, the relationship between mobility and receptance is

$$Y = \dot{X}/F = i\omega\alpha(\omega).$$

Inertance is the ratio of harmonic acceleration to harmonic excitation. Again for sinusoidal excitation, the relationship between receptance and inertance is

$$A = \ddot{X}/F = -\omega^2\alpha(\omega).$$

In this work the inertance was measured to determine the modal parameters. It should be pointed out that there is no loss of generality in assuming excitations having sinusoidal forms, because Any periodic function considered can be written as a Fourier Series and any aperiodic functions considered have a Fourier

Transform. For the current investigation of linear systems (principle of superposition applies), these properties allow us to study vibratory systems in this manner.

The damped SDOF system is an important case to study because any real system exhibits some form of damping. Damping introduces energy dissipation and phase difference between the output and the input. The equation of motion for the damped SDOF system is

$$m\ddot{x} + c\dot{x} + kx = f.$$

The damped SDOF system is shown in Figure 3. For f = 0, the equation of motion reduces to

$$m\ddot{x} + c\dot{x} + kx = 0.$$

A solution exists of the form

$$x = Xe^{st},$$

where s is a complex number. At this point a new parameter, ζ, the damping factor, will be introduced. The damping factor is the ratio of the damping in the system to the critical damping coefficient.

$$\zeta = c/c_{crit}$$

The critical damping coefficient is defined as

$$c = 2m\omega_n.$$

With this new parameter the equation of motion may now be written in the following manner

$$\ddot{x} + 2\zeta\omega_n\dot{x} + \omega_n^2 x = 0.$$

Substitution of our solution into the new equation of motion leads to an equation of new form. The new equation is a relationship between s and ζ. This equation gives two values of s for each value of ζ. This equation is written below.

$$s_{1,2} = [-\zeta \pm (\zeta^2 - 1)\ ]\omega_n$$

From this equation it can be seen that the parameter ζ influences the shape of the solution quite heavily. Four areas of interest exist in the domain of ζ. These are $\zeta = 0, 0 < \zeta < 1, \zeta = 1$, and $\zeta > 1$.

For $\zeta = 0$, the solution reduces to simple harmonic motion. For $0 < \zeta < 1$, s is complex. The real part of s is an exponentially decaying function and the imaginary part of s is an oscillatory function. Together they form an exponentially decaying function. This is known as underdamped motion. Underdamped motion oscillates at the frequency of damped vibration,

$$\omega_d = (1 - \zeta^2)\omega_n.$$

Figure 4 is an illustration of underdamped motion.

For $\zeta = 1$, s has double roots and the solution of the equation of motion is

$$x = (A + Bt)e^{i\omega t}.$$

The constants A and B are dependent upon the initial conditions. This case is known as critical damping. For this case, we see that the systems damping coefficient is equal to the critical damping coefficient. Generally the system will tend to the equillibrium position the fastest with critical damping. Figure 5 is an illustration of the critically damped case.

For $\zeta > 1$, the system is said to be overdamped. The parameter s is real and has two distinct values. The resulting motion is an exponentially decaying response. Figure 6 is an illustration of the overdamped case.

For $f \neq 0$, the results are similar to the undamped system. Again we let the force have the form

$$f = Fe^{i\omega t}$$

and assume a solution of the form

$$x = Xe^{i\omega t},$$

where X is a complex number and contains phase information. The equation of motion now becomes

$$(-\omega^2 m + i\omega c + k)Xe^{i\omega t} = Fe^{i\omega t}.$$

This results in the receptance FRF for the damped SDOF system having the form

$$\alpha(\omega) = 1/[\,(k - \omega^2 m) + i(\omega c)\,].$$

With the introduction of damping the FRF now has real and imaginary parts. This allows us to mathematically represent the phase difference between output and input. The relationship between the receptance FRF and the mobility/inertance FRF remain the same as those derived for the undamped case. Using the parameters ζ and ω_n we can write the receptance FRF in such a way that will help us analyze vibration measuring instruments. The receptance now takes the form

$$\alpha(\omega) = (1/k)/\,\{[1 - (\omega/\omega_n)^2] + i(2\zeta\omega/\omega_n)\}.$$

This may be written in complex exponential form as

$$\alpha(\omega) = |\alpha(\omega)|\, e^{i\phi},$$

where

$$|\alpha(\omega)| = (1/k)/\{[1 - (\omega/\omega_n)^2]^2 + (2\zeta\omega/\omega_n)\},$$

is the magnitude of the FRF and

$$\phi(\omega) = \tan^{-1}\{[2\zeta\omega/\omega_n]/[1 - (\omega/\omega_n)^2]\}.$$

is the phase angle of the FRF. Figure 7 is a plot of $|\alpha(\omega)|$ vs ω/ω_n and Figure 8 is a plot of ϕ vs ω/ω_n.

Defining resonance to be the frequency corresponding to the maximum amplitude of $|\alpha(\omega)|$, we see from Figure 7 that the degree of damping is most

important in this region. The resonant frequency can be shown to be

$$\omega_r = \omega_n(1 - 2\zeta^2).$$

For ω/ω_n near 1 and ζ approaching 0, the amplitude of the curve approaches infinity. Therefore, for light damping ($\zeta \Rightarrow 0$), ω_r is near ω_n and a small input will result in a large output. The phase diagram also exhibits some unique features. At $\omega/\omega_n = 1$ all the curves pass through 90°. When $\zeta = 0$, the curve has a discontinuity at $\omega/\omega_n = 1$. At this point the phase angle jumps from 0° to 180°. This means that for values of $\omega/\omega_n > 1$, the response is in the opposite direction of the excitation. These characteristics of the plotted FRF are helpful when plotting results from experimental data.

For damped systems we may define a quantity Q, known as the quality factor. Q is defined as

$$Q = |\alpha(\omega)|_{max}.$$

For lightly damped systems this can be shown to be

$$Q \simeq 1/2\zeta \simeq \omega_r/(\omega_2 - \omega_1),$$

where ω_2 and ω_1 are the frequencies corresponding to the half power points ($|\alpha|/\sqrt{2}$). This definition of Q will help us to determine the damping factor from experimental data.

Studying SDOF systems allows us to study the characteristics of vibration measuring instruments. In vibration testing a transducer is used to convert mechanical motion to a proportional voltage. The voltage signal can then be processed and displayed to give the experimenter information about the vibrating system. Signal conditioning and data display will be covered in more detail in the chapter describing the experiment. There are three basic vibration measuring instruments. These are instruments measuring accelerations, velocities, or

displacements. Force measurements are also done in modal testing. In this work it was acceleration and force that were measured. These were measured in order to calculate the inertance of the structure.

To measure acceleration a transducer called an accelerometer was used. To measure force a transducer called an impedance head was used. Detailed operation of these sensors will be covered in the next chapter. Here the equations of motion governing these instruments will be presented.

An accelerometer may be modelled as a SDOF system. The system is a case containing a mass, viscous dashpot, and a spring. A diagram of an accelerometer is shown in Figure 9. The equation of motion of an acceletometer is very similar to that of the forced SDOF system. From Figure 9 it can be seen that the equation of motion of an accelerometer is

$$m\ddot{z} + c\dot{z} + kz = -m\ddot{y}.$$

If we assume harmonic excitation of the base,

$$y = Ye^{i\omega t},$$

and a solution having the form

$$z = Ze^{i\omega t},$$

we can be show that for small values of ω/ω_n, the acceleration of the mass is proportional to the case. This means the acceleration of the mass is also proportional to the acceleration of the test structure. This is how the accelerometer mechanically measures the acceleration of the test structure. A plot of $|\alpha(\omega)|$ of the accelerometer shows the useful ranges of accelerometers. Figure 10 is such a plot. Notice for $\zeta = .70$, the curve is flat for values of $\omega/\omega_n \leq .3$. This indicates that for an instrument to measure acceleration it must have a damping factor in the neighborhood of .7. The accelerometer must also have a significantly

larger natural frequency than the measured frequency of interest. In fact, accelerometers do have a damping factor near .70. Accelerometers are made for many applications and it is their specific application which will dictate the design of its natural frequency.

2. Multi Degree of Freedom

MDOF systems are inherently more difficult to analyze then SDOF systems. As the number of degrees of freedom increase, the complexity of the problem increases even more. Despite this complexity, the study of MDOF systems is important because of their link between experimantal analysis and theoretical analysis. This can be best demonstrated by considering a continuous system as the limit of a MDOF system with an infinite number of degrees of freedom. This relationship is shown by Meirovitch [Ref. 13]. In principal the MDOF analysis can be carried out for a 2-DOF system and the same methods used can be applied to larger systems. This approach will be used to describe the methods used in MDOF analysis. However, many systems must be modelled using more than two degrees of freedom in order to get good experimental data. In this work the structure was modelled as a six degree of freedom system. Six degrees of freedom were chosen because measurements could be taken at approximateley equally spaced intervals along the structure corresponding to both nodes, antinodes, and points in between for the first five modes of vibration. This model of the structure resulted in the reciept of good experimental data for studying the first five modes of vibration. The first three modes are of interest because in many structures only the first few modes contribute significantly to the motion of the structure [Ref. 14]. As will be seen later each degree of freedom corresponds

to a measurement location. The free response analysis will be presented, followed by the forced response analysis.

We will begin with the undamped case. Figure 11 is an example of the undamped 2-DOF system. The equations of motion for this system are:

$$m_1\ddot{x}_1 + (k_1 + k_2)x_1 - k_2x_2 = 0$$

$$m_2\ddot{x}_2 - k_2x_1 + (k_2 + k_3)x_2 = 0$$

Already the equations of motion have become more cumbersome. Matrix notation and indicial notation are more compact methods for representing the equations of motion for MDOF systems generalized for any arbitrary degrees of freedom. For the remainder of this work these methods will be used to represent the MDOF equations of motion. In matrix form, the equations of motion are

$$\mathbf{M}\ddot{\mathbf{x}} + \mathbf{K}\mathbf{x} = \mathbf{0}.$$

Where $\mathbf{M}$ is the mass matrix, $\mathbf{K}$ is the stiffness matrix, $\ddot{\mathbf{x}}$ is the acceleration vector, and $\mathbf{x}$ is the displacement vector.

To solve the equations of motion for the MDOF system we will follow the same procedures as that used for the SDOF system. We will assume a solution of the form

$$\mathbf{x} = \mathbf{u}e^{i\omega t}.$$

Where $\mathbf{u}$ is the column vector of the displacement magnitudes. Substitution into the equation of motion and simplifying results in

$$\mathbf{K} - \omega^2\mathbf{M} = 0.$$

For this equation to have a nontrivial solution the determinant of this matrix must be zero.

$$|\mathbf{K} - \omega^2\mathbf{M}| = 0$$

This is the eigenvalue problem.

The eigenvalues are the natural frequencies of the system. The natural frequencies are designated ω_r, where r denotes the r^{th} mode of vibration. Associated with each eigenvalue is an eigenvector. Here, the notaton for the eigenvector is ψ_r.

The eigenvector describes the shape of the r^{th} mode of vibration. For this reason they are also called the mode shape vectors. The eigenvectors can be shown to be orthogonal with respect to the mass matrix. This orthogonality property results on the following relationships.

$$\Psi^T\mathbf{M}\Psi = \mathbf{M}_r$$

$$\Psi^T\mathbf{K}\Psi = \mathbf{K}_r$$

Where Ψ, the modal matrix, is an n x n matrix comprised of the eigenvectors. $\mathbf{M}_r$ is the diagonalized generalized mass matrix and $\mathbf{K}_r$ is the diagonalized generalized stiffness matrix.

The eigenvectors are unique in shape, but not in magnitude. A common practice in vibration analysis is to mass normalize the eigenvectors. This normalization is shown below.

$$\phi_r = (1/\sqrt{m_r})\psi_r$$

These are called the mass normalized eigenvectors. The new modal matrix, Φ, is an n x n matrix comprised of the orthonormal eigenvectors. The modal matrix now exhibits the following properties.

$$\Phi^T\mathbf{M}\Phi = \mathbf{1}$$

$$\Phi^T\mathbf{K}\Phi = \Omega_r^2$$

Where $\mathbf{1}$ is the diagonalized identity matrix and Ω_r^2 is a diagonalized matrix with the diagonal elements equal to the natural frequencies. Written in this form the modal matrix becomes a very powerful tool.

The equations of motion for the forced response of the MDOF system are:

$$\mathbf{M}\ddot{\mathbf{x}} + \mathbf{K}\mathbf{x} = \mathbf{f}.$$

We let $\mathbf{f}$ take the form

$$\gamma e^{i\omega t}.$$

Where γ is a column vector of force magnitudes. A second look at the equations of motion reveal that they are coupled. Our goal is to find a method to simplify their solution. Postmultiplying the $\mathbf{X}$ coordinates by the modal matrix Φ and premultiplying by each side of the equations of motion by Φ^T, we can uncouple the equations of motion. The new equations of motion are now

$$\ddot{\eta}_r + \omega_r^2 \eta_r = N_r,$$

where η_r are the generalized coordinates and N_r is the generalized force. We now have a set of n independent linear ordinary differential equations. These equations can be easily solved using well known methods. The uncoupling process also allows the systems to be treated as n uncoupled SDOF systems. That means the structure being tested in this work may be considered to be six uncoupled SDOF systems as opposed to one 6-DOF coupled system.

Another important use of the modal matrix is in the derivation of the FRF for the MDOF system. Following the approach used for the SDOF system analysis, we assume a solution of the equations of motion. This solution has the form

$$\mathbf{x} = \chi e^{i\omega t}.$$

This solution yields the result

$$\mathbf{x} = [\mathbf{K} - \omega^2 \mathbf{M}]^{-1} \mathbf{f}.$$

Defining the receptance FRF matrix to be

$$\alpha(\omega) = [\mathbf{K} - \omega^2 \mathbf{M}]^{-1},$$

we can write

$$\mathbf{x} = \alpha(\omega)\mathbf{f}.$$

The individual elements of the receptance matrix are defined to be,

$$\alpha_{ij}(\omega) = (x_i/f_j),\ f_m = 0;\ m = 1,n;\ \neq j.$$

The x_i correspond to response location locations. As pointed out earlier the structure in this work was modelled as a 6-DOF system. As a result there were six response locations for measurement on each structure. The expression above represents a similar expression derived for the receptance of the SDOF system.

Solving for the receptance matrix by inversion is not only tedious, but does not easily reveal the characteristics of the FRF. Using the modal matrix, we can show the receptance is

$$\alpha(\omega) = (\Phi\Phi^T)/(\omega_r^2 - \omega^2).$$

Each term in the FRF may now be calculated using this relationship.

$$\alpha_{ij} = \sum [({}_r\phi_i)({}_r\phi_j)]/(\omega_r^2 - \omega^2) = \sum [({}_r\psi_i)({}_r\psi_j)]/[m_r(\omega_r^2 - \omega^2)],$$

where ${}_r\psi_i$ is the i^{th} element of the eigenvector associated with the r^{th} eigenvalue and ${}_r\psi_j$ is the j^{th} element of this vector. Physically the i^{th} element of the r^{th} eigenvector is the displacement at the i^{th} response location for the r^{th} mode of vibration. A common way of writing this is

$$\alpha_{ij} = \sum ({}_rA_{ij})/(\omega_r^2 - \omega^2).$$

The term ${}_rA_{ij}$ is the modal constant. This form of the receptance is used when extracting modal parameters from experimental data. The same relationships exist between the receptance and the mobility/inertance as did for the SDOF case.

Analysis of the damped MDOF system is similar to the SDOF system. In this work a special type of damping called proportional damping was used to

model the damping characteristics of the structure. With proportional damping the damping is proportional to the mass matrix or the stiffness matrix or both. In this work the damping matrix was assumed proportional to the stiffness matrix. This relationship is shown below.

$$\mathbf{C} = \beta\mathbf{K}.$$

Where β is a real constant.

Proportional damping allows the use of the modal matrix to uncouple the equations of motion. The equations of motion for the free response analysis are

$$\mathbf{M}\ddot{\mathbf{x}} + \mathbf{C}\dot{\mathbf{x}} + \mathbf{K}\mathbf{x} = 0.$$

The damped natural frequencies of the system denoted by ${}_r\omega_d{}^2$, are

$${}_r\omega_d{}^2 = \omega_r{}^2(1 - \zeta_r{}^2),$$

where $\omega_r{}^2$ is the undamped natural frequency of the r^{th} mode and ζ_r is the damping factor for the r^{th} mode.

The forced response analysis of the structurally damped system results in the receptance FRF having the following form.

$$\alpha_{ij} = \sum [({}_r\psi_i)({}_r\psi_j)]/[(k_r - \omega^2 m_r) + i\omega c_r]$$

Proportional viscous damping is unique in the sense the eigenvalues are real and the mode shapes for the damped system are the same as for the undamped system. This expression for the FRF was used to extract the modal parameters of the structure.

Up to now we have not been concerned with the form of the forcing function in the forced response analysis. The only requirement has been that the function have a Fourier Transform. The forcing function used in this work will now be defined and the response analysis will follow. In this work an impact test was done on the structure. An impact test is done by imparting a force impulse to

the structure. A force impulse is defined as the time integral of the force.

$$F' = \int F\, dt$$

The force impulse is a force of relatively large magnitude occurring over a short period of time. The definition for F' requires that the integral have a finite value. As the time interval over which the force acts becomes smaller, the magnitude of the impulse approaches infinity. Even in this limit the integral must remain finite on physical grounds. When the magnitude of the impulse is equal to one and the time interval of the impulse is the infinitesimal time dt, the impulse becomes a unit impulse or delta function. The delta function is denoted by δ and has the following properties

$$\delta(t - \xi) = 0 \text{ for all } t \neq \xi,$$

$$\int_0^\infty \delta(t - \xi)\, d\xi = 1.0 \quad 0 < \xi < \infty.$$

With these properties we can multiply any function by δ and determine the value of that function where δ is defined. This operation is defined below.

$$\int_0^\infty f(t)\delta(t - \xi)d\xi = f(\xi)$$

To describe the response of a system to an impulse the undamped SDOF system will be used. This approach lends itself to an uncomplicated and very helpful solution to study when observing the response to impulse excitations. The analysis of the response to a unit impulse will be followed by the response to an arbitrary impulse. The structures in this work were excited with an arbitrary impulse. The frequency response analysis and the time domain analysis will presented. It will be seen that the computational difficulties encountered in the time domain analysis are what make the frequency domain analysis much easier to use.

A unit impulse acting on a body will impart to the body an initial velocity without any significant displacement change. This is seen by considering Newton's

second law. The force F is equal to m dv/dt, or F dt = m dv. For a unit impulse, 1/m = dv or x(0) = 1/m. Substitution of this initial condition into the equation for the displacement of the mass-spring system results in the solution

$$x = (1/\omega_n m)\, \mathrm{Im}\{e^{i\omega t}\}.$$

The response to a unit impulse is called the unit impulse response and is identified by the symbol h. For a delta of magnitude F' the response is simply

$$x = F'h.$$

Given the expression for the response to a unit impulse we can now determine the response to an arbitrary impulse. We can treat the arbitrary impulse as series of unit impulses and the response to each impulse as an impulse response delayed by the amount ξ. Analytically the response is given by the expression

$$f(\xi)\Delta\xi\, h(t - \xi).$$

A force impulse is shown graphically in Figure 12. Because we are considering only linear systems the principle of superposition holds. Therefore, we can sum together all the impulse responses and find the response to the arbitrary excitation. In the limit as $\Delta\xi$ approaches $d\xi$, this sum becomes an integral. The response to an arbitrary excitation is now defined by the integral

$$\int_0^t f(\xi)h(t - \xi)\, d\xi.$$

This integral is called the convolution integral. To evaluate this integral the analytical form of the forcing function and the unit impulse response of the system must be known.

From the analysis of MDOF systems it was found that through the modal matrix the equations of motion could be uncoupled and treated as n different SDOF systems. For a MDOF system subject to an arbitrary impulse n different convolution integrals must be solved. Unless the transformed forcing function is an

easily integrable function this is an extremely difficult task. However, if we treat the same problem in the frequency domain, the evaluation of difficult integrals is replaced by simple multiplication.

Earlier in the SDOF anlysis section the equation of motion for SDOF system was solved using the Fourier Transform method. The result was a function called the transfer function. The transfer function was defined as the ratio of the Fourier Transform of the output to the Fourier Transform of the input. This ratio is written in the following manner

$$H(\omega) = X(\omega)/F(\omega).$$

From this expression we see that the product of the transfer function and the Fourier Transform (FT) of the forcing function is equal to the FT of displacement. A relationship exists between convolution in the time domain and multiplication in the frequency domain. If we begin with the convolution integral and compute its FT we see that the transform is equal to the product of two functions. One of the functions is the FT of the forcing function and the other is the FT of the impulse response. Remembering that the convolution integral is equal to the displacement x, it can be seen that the FT of the displacement is equal to the product of the FT of the impulse response and the FT of the forcing function.

$$\mathcal{F}\{x\} = \mathcal{F}\{f * h\} = X(\omega) = F(\omega)H(\omega)$$

The symbol $\mathcal{F}\{\}$ denotes the Fourier Transform of the expression in parentheses. Dividing $X(\omega)$ by $F(\omega)$ we see that the FT of the impulse response is equal to the transfer function of the system. It can now be seen that the analysis of the response of a system to an arbitrary impulse is much simpler in the frequency domain. The response of an MDOF system to an arbitrary impulse can now be found by summing together the product of the forcing function and the system

transfer function for each mode of vibration. This is in fact how the FRF of the structure is found. Earlier the relationship between the FRF and the transfer function was shown for an SDOF system. This concept can be further extended to the n uncoupled equations of motion for the MDOF system.

In impact testing the system response is a decaying sinusoid. Figure 13 is an example of the response to an arbitrary impulse. During testing of the structure over 100 impacts were made on the structure and their responses measured. The form of the exciting function was not known, but with the use of a signal analyzer its signal was discretized and a discrete Fourier Transform (DFT) of the impulse found. The DFT of the input will show the spectral characteristics of the impulse. As will be seen in the Experimental Procedures chapter it is the spectral characteristics of the impulse which will be used to determine the FRF of the structure. Figure 14 is an example of some impulse functions and their spectral representations.

C. CONTINUOUS SYSTEMS

In this section an equation will be derived which will predict the frequency of flexural vibration for the test structures. The geometry of the test structures and the relevant equations will be presented followed by the derivation of the frequency equation. The section will conclude with a comparison of the derived equation to results obtained using shell theory.

The test structure was a thin cylinder with circular cross section. The convention followed by Whitney [Ref.15] will be used to describe the coordinate system and displacements of the elemental section of the test structure. This convention is shown in Figure 15. The thickness is denoted by h, length by a, and width by b. The radius to the reference surface (midplane of the thickness) is

denoted by R. The x coordinate is along the length of the tube, s along the circumference, and z is in the thickness direction. Displacements u, v, and w correspond to displacements in the x, s, and z directions respectively. The field equations (equilibrium, strain-displacement, and constitutive) and laminated plate theory will be used to derive the equation of motion of the test structure. From this equation the equation for the flexural vibrations of the test structure will be derived. We are interested in deriving a simplified equation similar to the equation derived from the Euler-Bernoulli beam theory. Essentially we are going to treat a two dimensional laminated shell as a one dimensional homogeneous beam. The field equations of interest are presented below.

The equilibrium equation in indicial notation is

$$\partial_i \sigma_{ij} + X_j = \partial^2 u_j / \partial t^2 .$$

Strain-displacement relations for curved surfaces are derived by Timeshenko [Ref. 16] and are given below.

$$\epsilon_x = \partial u / \partial x$$

$$\epsilon_s = [R/(z+R)] \partial v / \partial s + w/R$$

$$\epsilon_{xs} = \partial v / \partial x + [R/(z+R)] \partial u / \partial s$$

The parameter R is the radius to the reference surface. In this work the reference surface was the midplane of the laminate. Stresses in a body are a function of the applied forces and moments. The strain in a body is a function of geometry. These equations are kinematical relations between strain and displacement, they are independent of the material properties of the body. What relates stress to strain in a body are the unique properties of the body's material. This relationship is called the constitutive relationship. In indicial notation this is written as

$$\sigma_{ij} = C_{ijkl} \epsilon_{kl},$$

where C_{ijkl} is the fourth order stiffness tensor. This relationship may also be written in the inverted form

$$\epsilon_{ij} = S_{ijkl}\sigma_{kl}$$

where S_{ijkl} is the fourth order compliance tensor. Tsai [Ref. 17] demonstrates how these equations can be reduced using a contracted notation. The contracted constitutive relations are

$$\sigma_i = C_{ij}\epsilon_j$$

$$\epsilon_i = S_{ij}\sigma_j$$

where the equations are written in contracted form. The stiffness and compliance terms no longer have their tensor properties , but now lend themselves to matrix operations. The compliance matrix is the inverse of the stiffness matrix. With these relations presented we are now ready to proceed with the derivation of the flexural vibration equation.

By starting with the equation of motion derived by Whitney for a curved laminated plate and following the same approach used by Whitney, a one dimensional equation of motion for the transverse vibrations of the test structure will be derived. Whitney's assumptions will be presented followed by the derived equation of motion.[Ref. 15]

1.The plate is constructed of an arbitrary number of 2 - D anisotropic layers bonded together. The orthotropic axes of material symmetry , however, of an individual layer need not coincide with the x-s axes of the cylindrical plate.

2. The plate is thin, i.e., the thickness h is much larger then the other physical dimensions.

3. The displacements u,v, and w are small compared to the plate thickness.

4. Inplane stresses ϵ_x, ϵ_s, and ϵ_{xs} are small compared to unity.

5. The radius of the plate R is much smaller than the thickness h.

6. In order to include inplane force effects, the nonlinear terms in the equations of motion involving products of stresses and plate slopes are retained. All other nonlinear terms are neglected.

7. Transverse shear strains ϵ_{xz} and ϵ_{sz} are neglected.

8. Tangential displacements u and v are linear functions of the z coordinate (Kirchoff-Love hypothesis).

9. The transverse normal strain ϵ_z is negligible.

10. Each ply obeys Hooke's law.

11. Rotary inertia terms are negligible.

12. There are no body forces.

13. Transverse shear stresses σ_{xz} and σ_{sz} vanish at the surfaces $z = \pm h/2$.

Using these assumptions the equation of motion for the transverse motion is:

$$\partial^2 M_x/\partial x^2 + 2\,\partial^2 M_{xs}/\partial x \partial s + \partial^2 M_s/\partial s^2 - N_s/R + N_x\,\partial^2 w/\partial x^2$$
$$+ 2\,N_{xs}\,\partial^2 w/\partial x \partial s + N_s\,\partial^2 w/\partial s^2 + p = \rho\,\partial^2 w/\partial t_2.$$

For purposes of the experiment the following additional assumptions are made which further simplify the equation of motion.

14. $M_{xs} = M_s = N_s = N_{xs} = p = 0$

15. $\rho = h\rho_o$

Where M_{xs} and M_s are the moment resultants, N_{xs} and N_s are the stress resulatants, and p is the surface stress resultant from classical plate theory. The term ρ_o is the mass density per unit volume of the test structure. With these assumptions the equation of motion reduces to

$$\partial^2 M_x/\partial x^2 = h\rho_o\,\partial^2 w/\partial/t^2.$$

From laminated plate theory the constitutive relations are

$$\mathbf{N} = \mathbf{A}\epsilon + \mathbf{B}\kappa$$

$$\mathbf{M} = \mathbf{B}\epsilon + \mathbf{D}\kappa$$

Where $\mathbf{N}$ is the column vector of the stress resultants, $\mathbf{M}$ is the column vector of the moment resultants, and $\mathbf{A}$, $\mathbf{B}$, $\mathbf{D}$, are the modified stiffness matrices, see Jones [Ref. 18] for a definition of these matrices. For $\mathbf{N} = \mathbf{0}$, these equations reduce to

$$\mathbf{M} = [\mathbf{D} - \mathbf{B}\mathbf{A}^{-1}\mathbf{B}]\kappa.$$

The moment curvature relationship is now

$$\kappa = \mathbf{d}^{*}\mathbf{M}.$$

Where κ is the column vector of the curvatures and $\mathbf{d}^{*}$ is the inverse of the bending stiffness matrix. The expanded bending stiffness matrix may be found in Jones [Ref. 18]. The relationship between the curvatures and displacement w are

$$\kappa_x = -\partial^2 w/\partial x^2,$$

$$\kappa_s = -\partial^2 w/\partial s^2,$$

$$\kappa_{xs} = -2\,\partial^2 w/\partial x \partial s.$$

From assumption 14 it can be seen that the curvatures are only related M_x. At this point the transverse displacement w is still a function of x, s, and t. One more assumption is needed to further reduce the equation of motion. This assumption is given below.

16. The displacements due to d_{12}^{*} and d_{16}^{*} are negligible compared to the displacements due to d_{11}^{*}.

The result of assumption 16 is that the displacement w can now be written as a function of x and t only. For constant d_{11}^{*} the moment- curvature relation is now

$$-1/d_{11}^{*}\,\partial^2 w/\partial x^2 = M_x$$

Substituting this relationship into the equation of motion results in the familiar

Euler-Bernoulli beam equation

$$-1/d_{11}{}^{*}\partial^4 w/\partial x^4 = h\rho_0\partial^2 w/\partial t^2.$$

Assuming a solution of the form

$$w = w(x)e^{i\omega t},$$

time can be eliminated from the equation of motion. The resulting equation is a statement of the eigenvalue problem for continuous systems.

$$d^4 w/dx^4 - h\rho_0\omega^2 d_{11}{}^{*}w = 0$$

The solution to this problem results in an infinite set of values for the parameter ω^2 called the eigenvalues. The eigenvalues correspond to the natural frequencies. If we define β in the following manner then ω will be a function of β, β will depend on the boundary conditions.

$$\beta^4 = h\rho_0\omega^2 d_{11}$$

The relationship between β and ω is

$$\omega_n = (\beta_n l)^2 \sqrt{1/(h\rho_0 d_{11}{}^{*}l^4)}.$$

The values of $\beta_n l$ are dependent upon the boundary conditions. In this experiment the test structure was subject to clamped-free boundary conditions. The values of $\beta_n l$ for the first three modes of vibration are given below.

$$\beta_1 l = 1.875$$

$$\beta_2 l = 4.694$$

$$\beta_3 l = 7.855$$

Comparison of the derived equation to the equation for a homogenous isotropic beam reveals a striking similarity. The frequency of vibration for a homogeneous beam is given by the following equation derived from Euler-Bernoulli beam theory.

$$\omega_n = (\beta_n l)^2 \sqrt{EI/ml^4}$$

Where E is Young's modulus of the material, I the area moment of inertia of the structure, m the mass per unit length and l the length. The eigenfunctions, more commonly called the normal modes, are the same as predicted from the Euler-Bernoulli beam theory. The normal modes of vibration are

$$W_n(x) = A_r[(\sin\beta_n l - \sinh\beta_n l)(\sin\beta_n x - \sinh\beta_n x) + (\cos\beta_n l + \cosh\beta_n l)(\cos\beta_n x - \cosh\beta_n x)].$$

The magnitude of A_r is such that it satisfies the orthogonality condition

$$\int m(x)\, W_m(x)\, W_n(x)\, dx = 0,$$

where m(x) is the mass per unit length. This completes the derivation using the two dimensional laminated plate theory.

The presentaion given above has assumed that a shell could be treated as a plate and in turn the plate treated as a beam. What follows is a justification of the approach taken using results given by Donnell. A detailed description of shell theory and the associated assumptions will not be presented. Instead, a qualitative explanation of the highlights of the theory pertinent to this work will be given. This method is more in the spirit of this work.

The most general type of structure is the shell. A plate is a special case of a shell and a beam a special case of a plate. Exact solutions to the field problem given by three dimensional elasticity are limited to certain special cases. In these cases the equations are quite cumbersome and often not readily usable without the aid of a computer. Shells are structures in which one dimension, the thickness, is much smaller than the other two dimensions. This smaller third dimension has less resistance to transverse displacement. It is these transverse displacements or deflections with which we are mainly concerned. The Kirchoff-Love hypothesis (straight lines normal to the midplane remain straight, normal to the

midplane, and unchaged in length after deformation) simplifies the problem and allows us to treat the real life three dimensional problem as a two dimensional problem. With this assumption the two dimensional shell theory equations of motion are governed by eighth order partial differential equations. These equations require four boundary conditions along each edge of the structure. For the case of a circular cylinder the solutions to the equations of motion can be found in closed form. Even though this geometry is a special case of the general shell theory its usefulness is quite obvious.

The general solution to the equations of motion for the circular cylindrical shell is a double series solution. Hence tranverse displacements are governed by the integer values of m and n, where m and n are the summation indices. The solution is dependent upon the boundary conditions and will be harmonic functions in m and n. Both m and n have physical interpretations. The value of m is the number of axial half waves and n is the number of circumferential whole waves. Corresponding to this are the circumferential modes of vibration and the axial modes of vibration. An example of these can be seen in Figures 16 and 17. The values of m go from 1 to ∞ and the values of n go from 0 to ∞.

The modes excited will depend upon the force used to excite the structure. Experience has shown that for values of $n \geq 2$, the frequencies of vibration are much higher than the lowest frequencies of vibration of a cylinder. For $n = 0$, the cylinder may be treated as a membrane in certain special cases. A value of $n = 1$ is usually associated with the lower frequencies of vibration. However, for this to be true we must investigate the form of the forcing function and the values of m. If the value of the half wave length of the forcing function, that is the distance between nodes if the forcing function is written as a sum of sines and cosines, is

much greater than the diameter of the cylinder, than the cylinder may be treated as a beam for certain values of m. If the wavelengths corresponding to the value of m is much larger than the diameter of the cylinder, than the cylinder may be treated as a beam. A detailed mathematical description of these results is given by Donnell.[Ref. 19]

In this investigation the forcing function was a force impulse. The ideal impulse contains all frequencies of equal magnitude. However, the ideal impulse is not achievable in the laboratory. The second (II) and third curves (III) in Figure 14 give a representative look at the types of spectra seen in this work. The magnitude of the frequencies above 500 Hz is small compared to the magnitude of the frequencies below 500 Hz. This would seem to indicate for the structures tested in this work, the participation of modes with frequencies higher than 500 Hz were negligible compared to the modes below 500 Hz. The half wavelengths of the frequencies required to excite the first three modes are on the order of the length of the tube. Therefore, the treatment of the of the test structures as beams was justified.

III. EXPERIMENTAL PROCEDURE

A. INTRODUCTION

The introduction to this work has answered why we need to investigate the modal parameters of a lightweight composite structure. The theoretical background presented has given us insight into the theoretical analysis behind our investigations. The experimental section will now present the "hows" of the investigation.

The objective of the experiment was to determine natural frequencies and mode shapes of a composite tube with clamped-free (cantilevered) boundary conditions. Designing the experiment included selection of sensors, selection of instrumentation, set up of the test area, verification of instrument specifications, determination of test procedures, and determination of a method for the analysis of the data. The remainder of this chapter will cover these topics in detail.

B. STRUCTURES

Both aluminum and composite structures were studied. The aluminum specimens had four different cross sections. The cross sections were rectangular, circular, a square shell, and a circular shell. Figures 18 through 21 illustrate these cross sections. In these figures l is the length, d is the depth, and b is the width. The width of each specimen was kept constant throughout the testing. However, the length of each specimen was varied in order to test different l/d ratios. Different l/d ratios were stucied as a check on the range of applicability of the beam frequency equation. Table 1 shows the area moments of inertia, the cross sectional areas, lengths, and l/d ratios tested for each specimen. Also included in

this table is the value for the Young's modulus of aluminum and the density of aluminum. During testing the specimens were subject to clamped-free boundary conditions. The equation used to predict the natural frequencies of the aluminum specimen was the Euler-Bernoulli frequency equation. This equation is

$$f_n = [(\beta_n l)^2/2\pi]\sqrt{(EI)/(\rho A l^4)},$$

where A is the cross sectional area and ρ is the mass per unit volume.

The composite specimens tested were thin graphite/epoxy tubes, of circular cross section. The tubes were made with Fiberite prepreg FX-13F76 and were filament wound. The lamina stacking sequence in the first tube was $[90,\mp 60_3,90]$. This tube measured 129 cm long, with an inner diameter of 3.76 cm and an outer diameter of 4.17 cm. Tube weight was 5.28 N. The lamina stacking sequence in the second tube was $[90,\mp 45_3,90]$. This tube measured 107 cm long, with an inner diameter of 3.81 cm and an outer diameter of 4.27 cm. Tube weight was 4.78 N. Material properties used in the calculation of the stiffnes matrices and frequencies are shown in Table 2. Also included in Table 2 are the linear combinations of the unidirectional stiffnesses. The linear combinations are used to calculate the transformed stiffnesses for angle plies. For a definition of the linear combinations see Tsai [Ref. 20]. Table 3 shows the tube geometry and lay up for the tube 1 and Table 4 shows the geometry and tube lay up for tube 2. The transformed stiffnesses for each angle ply are shown in Table 5 for tube 1 and in Table 6 for tube 2. Refer to Tsai [Ref. 20] for the calculation of the transformed stiffnesses using linear combinations. From the transformed stiffnesses the **A**, **B** and **D** matrices, described in the previous chapter, were calculated. The method used to calcualte these matrices is described by Tsai [Ref. 20]. Calculations following this method were then carried out on a spreadsheet. Table 7 shows the values of the

$\mathbf{d}^*$ matrix (see previous chapter) for tube 1 and Table 8 shows this matrix for tube 2. Table 9 shows the values of the predicted frequencies for tube 1 and Table 10 shows those for tube 2. In order to use the equation derived in the previous chapter we must apply a geometric correction factor. This is applied because now we are treating tubes not rectangular beams. The correction factor is the ratio between the radius of gyration squared of a tube and the radius of gyration squared of a rectangular beam. This is just like using different moments of inertia and areas in the Euler-Bernoulli equation for isotropic beams. This correction factor is given below.

$$K = (6R^2)/(h^2)$$

Substitution of this factor into the frequency equation gives the result

$$f_n = (\beta_n l/2\pi)\sqrt{(6R^2)/(h^3 d_{11}^* \rho_0 l^4)}$$

This was the equation used to predict the frequencies of the composite tubes.

C. SENSOR SELECTION

As pointed out in the previous chapter, a transducer called an accelerometer was used to measure acceleration and a transducer called an impedance head was used to measure the applied force. Both of these instruments are piezoelectric sensors. The piezoelectric sensor takes advantage of a unique property of quartz crystals. When a force is applied to the crystal an electric potential is present across the face of the crystal. This potential is proportional to the applied force. Modern day piezoelectric sensors come in two types: charge and voltage. Both types measure forces and motion using the piezoelectric effect, but differ in the way the voltage signal is transmitted. A charge type sensor consists of the quartz crystal and a mass (called the seismic mass) enclosed in a case. Attached to

opposite faces of the crystal are leads which carry the high impedance voltage signal. A voltage type sensor consists of the quartz crystal, seismic mass, and a built in microelectronic charge amplifier. The function of the charge amplifier is to convert the high impedance voltage signal to a low impedance voltage signal. Sensor sensitivities are measured in in millivolts (mV) per engineering unit (g's or Newtons (N)).

The advantages of the charge type sensor are simplicity of design, and reliability. The sensitivity of the sensor is dependent upon the seismic mass and the size of the crystal. The larger the the sensor the more sensitive the sensor is. This is a disadvantage if the measured signal is small (< 10 mV) and the test structure is lightweight. Charge type sensors also require special low noise cables when measuring small output signals.

Voltage type sensors are good for measuring small signals from lightweight structures. They can be made lighter in weight in order to have a negligible mass damping effect upon the structure. Low noise cable is not required for these sensors. However, the voltage type sensors are more complicated to manufacturer and tend to be more expensive than charge type sensors. Sensors may be attached to the test structure in a number of ways. The three basic methods of attachment are by stud, adhesive, or wax.

The weight of the sensors, the method of attachment, and sensitivity were the most important criterion in selecting accelerometers for the experiment. The priority in choosing the accelerometers was their weight. Typical accelerometers weigh close to one half Newton and have sensitivities from 50 mV/g to 100 mV/g. For this experiment accelerometers with a weight of .05 N or less were desired. This size accelerometer would have a neglible mass damping effect upon the

structure. Sensitivities of 5 mV/g or greater were required because the excitation forces and resulting accelerations were small. Sensitivities any less than this value would bring the signal down into the noise level. This sensitivity is very high for accelerometers of such low weight. The standard accelerometer would not do the job. Attachment of the sensors to the structure could not be allowed to appreciably change the stiffness characteristics of the structure. Therefore, it was decided that the accelerometers must be attached by wax. In addition to these requirements the accelerometers needed to exhibit good frequency response from 5 Hz to 1KHz. This frequency range includes the first five modes of vibration of the tube.

In modal tests a modal hammer is used to impart a force impulse to the test structure. For this work a modal hammer was not available. In order to excite the structure with an impulse and measure this input, an impedance head was chosen and modified to act as a modal hammer. An impedance head is a piezoelectric transducer with a force transducer at one end and an accelerometer at the other end. A force transducer consists of a piece of piezoelectric material, in this case quartz, enclosed in a case. A force applied to the transducer creates a potential proportional to the applied force. This is how force measurements were made. To make a modal hammer a stud was attached to the force transducer end of the impedance head. Striking the structure with the exposed end of the stud produced an acceptable pulse as seen on an oscilloscope. The impedance head sensitivity requirements were not as important as those for the accelerometers. This is because the impedance heads interaction with the structure did not change the mass or stiffness characteristics of the structure. However, the frequency response of the impedance head did have to be approximately flat from 5 Hz to 1KHz.

As the modified modal hammer a Piezotronics Mechanical Sensor (Model 288A11) was used to measure force. The impedance head had a nominal sensitivity of 232.5 mV/N. Accelerometers with integratied microelectronic amplifiers were chosen because they offered low mass, high sensitivity, and good frequency response. The one chosen was a Piezotronics Quartz Accelerometers (Model 309A). The accelerometers had a nominal sensitivity of 5 mV/g.

D. INSTRUMENTATION

The next step in conducting the experiment was to choose instrumentation for signal conditioning and signal analysis. For signal conditioning (power sources for the microelectronic amplifiers and secondary signal amplification) Piezotronics Dual Mode Charge Amplifiers (Model 464A) were chosen. These amplifiers were used for both the impedance head and the accelerometers. These units provided sufficient power to the amplifiers and also allowed amplification of the input signals from the sensors.

For signal analysis a Spectral Dynamics SD380 signal analyzer was used. The signal analyzer is a microprocessor based analog to digital converter. The signal analyzer samples the the incoming voltage and then computes a Fast Fourier Transform (FFT) of the waveform. The signal analyzer can produce a time representation of the waveform (similar to a digital oscilloscope), a frequency representation (waveform spectrum), statistics of the waveform (pdf, cdf, etc.), a power spectrum, Inverse Fast Fourier Transform (IFFT), and compute a transfer function (TF). As shown in the previous chapter the FRF and the TF are of the same form and represent the same information. The FRF measured in this experiment was the inertance. The parameters will be extracted from the TF.

Before the method of calculating the TF is defined, the FFT characteristics of the signal analyzer will be presented. The signal analyzer has a 12 bit analog to digital converter. Sampling rate was controlled by three factors. These were the number of lines of resolution desired, the maximum value of the frequency scale, and the number of points per transform. The number of lines of resolution determines the Δf of the frequency scale (Ex. 400 lines of resolution means the frequency scale will be divided into 400 equally spaced frequency intervals from 0 Hz to the maximum chosen frequency). An example best shows how to deteremine the sampling rate. The operator begins by choosing the the number of lines of resolution and the maximum frequency. The signal analyzer has a predetermined number of points per transform corresponding to the number of lines of resolution chosen. For this example the max frequency is 1000 Hz and the number of lines of resolution is 400. The corresponding number of sample points per transform is 1024. Begin by dividing f_{max} by the lines of resolution. This will give the fundamental frequency of the Fourier Series representation of the sampled waveform.

$$\Delta f = 1000/400 = 2.5 \text{ Hz}$$

The reciprocal of this is taken to find the transform period.

$$T = 1/\Delta f = .4 \text{ sec}$$

Dividing the points per transform by the transform period will result in the sampling rate.

$$1024/.4 = 2056 \text{ samples/sec}$$

This is the sampling rate for this example. The sampling rate may be varied by changing the maximum frequency or the number of lines of resolution.

When operated in the TF role, the signal analyzer displays both the magnitude of the TF and the phase of the TF. As shown in the previous chapter, force and acceleration measurments were needed to calculate the TF (inertance). Therefore, two inputs to the signal analyzer were required. These inputs were the voltage signal from the impedance head (force measurement) and the voltage signal from an accelerometer (acceleration measurement). The signal analyzer had four channels for input, however only two channels were used. Channel A was used for input from the impedance head and channel B was used for the inputs from the accelerometers. In this arrangement a TF was computed between channels B and A.

Experimentally determining the TF requires more than taking the ratio of the output to the input at different frequencies. This is due to the presence of noise and the randomness of the input signals. The data computed from the FFT of the sampled waveforms can still be used to calculate the TF. This is done using the autocorrelation function and its Fourier Transform, the auto spectral density; and the cross correlation function and its Fourier Transform, the cross sprectral density. These quantities are defined below.

$$R_x(\tau) = E[x(t)x(t+\tau)]$$

$$R_{fx}(\tau) = E[f(t)x(t+\tau)]$$

$$S_x(\omega) = \mathcal{F}\{R_x(\tau)\}$$

$$S_{fx}(\omega) = \mathcal{F}\{R_{fx}(\tau)\}$$

E[ ] denotes the expected value of the function in the brackets. The autocorrelation is a method of finding periodicity in a signal. The cross correlation compares signals and enables us to find similarities between them. The use of

these functions in determining a TF would require the solution of difficult integral equations. It is in this light that their Fourier Transforms become extremely useful.

Beginning with our basic definitions of the TF and of the auto/cross sprectral densities, we can derive what are known as the Weiner-Khinchine relationships. The Weiner-Khinchine relationships are:

$$H(\omega) = S_{fx}(\omega)/S_f(\omega) = S_f(\omega)/S_{xf}(\omega).$$

The first relationship is the relationship used by the signal analyzer to compute the TF. A detailed explanation of how the auto spectral density and the cross spectral density are computed from the sampled waveforms is given by Newland [Ref. 21]. The auto sprectal density and cross spectral density are complex functions of frequency. Therefore, the TF is also a complex function of frequency (we already found this to be true in our theoretical analysis). The magnitude and phase angle of the TF were found using the following equations:

$$|TF| = [\sqrt{Re\{S_{fx}\}^2 + Im\{S_{fx}\}^2}] / S_f$$

$$\phi = \tan^{-1} [Im\{S_{fx}\}/Re\{S_{fx}\}].$$

One measurement alone is not used to calculate the magnitude and phase of the TF. The signal analyzer takes many measurements of the input signal and averages these measurements. The method of averaging used in this experiment was the sum method of averaging. The signal analyzer computes a FRF from the first measurement. After making a new measurement, the arithmetic mean of the real parts of the spectral densities of the two measurements is calculated. The arithmetic mean of the imaginary parts is also calculated. From these mean values a new TF is computed. These mean values are then stored in memory. This procedure was repeated between the values in memory and the newly measured values until the pre set number of measurements were made. The number of

measurements made is called the count. The number of counts required to get smooth FRF plots is determined empirically. In general, a greater number of counts were required for large bandwidth tests as compared with small bandwidth tests. For this experiment the number of counts used was 10. This number was chosen because this number of averages gave excellent FRF plots.

E. CALIBRATION

To ensure good data during the experiment, the manufacturer's specifications for the instrumentation required verification. The instruments requiring verification were the signal analyzer and the amplifiers. Verification of sensor sensitivities was also done.

The frequency response of the signal analyzer was the performance parameter which required verification. The signal analyzer was rated to measure the amplitude of the input signal to ± .5 dB over its entire operational frequency range (0 Hz - 40 KHz). This response was verified by simulating acceleration measurements and inputting them to the analyzer.

The signal analyzer was set up to operate in its waveform spectrum mode. The simulated acceleration measurement was generated by a Wavetek 20 MHz Pulse/Function Generator. The signal output by the Wavetek was a sinusoid of varying frequency. The frequency varied from 1 Hz to 10 KHz for the verification test. The signal was input to each channel of the signal analyzer and the measured amplitude recorded. A LeCroy 9400A Dual 175 MHz digital oscilloscope recieved the same input signal as each channel of the signal analyzer. In this manner, the measurements made by the signal analyzer could be directly compared to those made by the digital oscilloscope, which is calibrated against an NIST (National Institute for Standards and Technology) source by the manufacturer. secondary .

Running two verification tests in this manner showed the signal analyzer measured the input better than ± .5 dB over the tested frequency range. These results indicated that the signal analyzer would give good frequency response in the frequency range of interest (5 Hz - 1 KHz).

The frequency response of the amplifiers were rated at ± 5% of the full scale input signal over a frequency range of near DC to 100 KHz. To check this specification a similar test was run as done for the signal analyzer. A signal with amplitude 10 mV was input to each amplifier. The amplifier gain was set to 50 and the output signal from the amplifier was measured on an analog oscilloscope (Tektronix 465 M). The frequency of the input signal varied from 1 Hz to 10 KHz. The tests showed the amplification provided by the amplifiers was better than ± 5% of the full scale input signal. These results indicated the amplifiers were performing satisfactorily.

Verification of sensor sensitivities was conducted using an Endevco Model 2270 piezoelectric calibration accelerometer. The reference (Endevco) accelerometer was attached to an aluminum block attached to a shaker. Each test accelerometer was also attached to the aluminum block. Attachment was done using wax. The appropriate sensitivity settings and amplification settings were made on the amplifiers for each accelerometer. The shaker was then turned on and the gain adjusted. The acceleration measurements made by each accelerometer were then recorded as the shaker frequency ranged from 5 Hz to 1 KHz. This procedure allowed the verification of accelerometer sensitivities and their nearly flat (< 3% amplitude deviation) frequency response. The verification tests showed that the sensitivities of the accelerometers were within 1% of the values given by manufacturer. The verification tests also showed that the accelerometers

did exhibit a nearly flat frequency. A copy of the Calibration certificate for the accelerometer used in the testing is given in Appendix C.

Similar tests were conducted on the impedance head. Tests results showed the impedance head sensitivity was within 1% of that given by the manufacturer. The tests also verified the near flat frequency response of the impedance head. A copy of the calibration certificate for the impedance head is in Appendix C.

F. TEST PROCEDURES

During testing the aluminum structures were supported by clamps and a vise. The aluminum structures were modeled as two degree of freedom systems. This model was chosen because only the fundamental frequency was of interest. The test procedures followed on each aluminum structure were the same. The procedures for the tests done on the rectangular cross section will be described. The test piece was clamped in place for the first l/d given in Table 1. The accelerometer was placed at the end of the test piece and was used as the reference coordinate. The location half way between the cantilever and the accelerometer was marked and used as the response location. The test piece was struck at the response location ten times with the modal hammer. Ten was used because this number of averages on the analyzer gave good FRF plots. When the analyzer was done averaging the data, the data was transferred to a Compaq 386/20 personal computer for analysis. The analyzer was then cleared and these procedures were repeated for each l/d ratio and cross section

During testing the composite structures were supported with a clamping mechanism machined from aluminum. Figure 22 is a photograph of the test setup. Test procedures for both tubes were similar. A total of six tests were done on tube 1 and eleven tests on tube 2. The procedure for testing tube 1 will be

described followed by the procedures for testing tube 2 in some detail since more degrees of freedom were used than for the aluminum specimen. This is because mode shapes and higher mode frequencies were desired in the case of the composites. Each degree of freedom corresponded to a measurement location. The degrees of freedom were located at .20 m, .40 m, .60 m, .80 m, and 1.29 m from the cantilever. Figure 23 is an illustration of the location of the degrees of freedom. The numbers above the arrows in Figure 23 indicate the degree of freedom/response coordinate of that location.

For all the tests the accelerometer was used as the reference coordinate. The accelerometer was placed at location four. These tests were done to extract the first three modes. The testing was done by striking the tube ten times at each response coordinate. After ten impacts had been averaged on the analyzer the data was transferred to the PC. The signal analyzer was then cleared and the these procedures were repeated until each response coordinate had been impacted ten times. Therefore, one test comprised of 60 impacts on the structure. In each test there were five transfer mobility measurements (response coordinate and reference coordinate at different locations) and one point mobility measurement (response coordinate and reference at the same location). Test two was simply a repeat of test one. This was done in order to verify the data taken in test one.

The degrees of freedom for tube 2 were located at .16 m, .32 m, .48 m, .64 m, .80 m, and 1.07 m from the cantilever. Figure 24 is an illustration of the location of the degrees of freedom. For all the tests the accelerometer was used as the reference coordinate. The procedures followed in testing the second tube were the same as for the first tube except the location of the accelerometer was not limited to location four and a greater number of tests were conducted. The first five

frequencies of the second tube were measured. For five tests the accelerometer was placed at response location four. The accelerometer was placed at location three for four tests and at location five four two tests. Varying the location of the reference coordinate allowed the measurements to be cross checked.

Once the data had been transferred to the PC from the signal analyzer, a modal analysis software package was used to extract the modal parameters. The software package used in this work was EMODAL-PC v.2.75 by Entek. The software utilized a least squares circle fit of the data to extract the modal parameters. A description of the least squares circle fit is given by Ewins [Ref. 22].

IV. RESULTS AND DISCUSSION

A. INTRODUCTION

In this chapter the results of the experiment will be presented. Numerical results will be presented in table and bar chart format and include a comparison of the predicted frequencies with those found in the experiment. Also included are a sample of the first three measured mode shapes and the predicted mode shapes for these modes. In addition, the test results for the aluminum structures will be presented. The results obtained for these structures were used for qualitative comparison to the results obtained for the composite structures. The chapter will conclude with a brief discussion of the results.

B. RESULTS

Table 11 is a presentation of the test results for the aluminum test pieces. Figures 25 through 28 are bar charts of percent error versus aspect ratio for each different cross section of aluminum. The percent error is defined as

$$\% \text{ Error} = [1 - (\text{MEASURED FREQ/PREDICTED FREQ})].$$

The results for the rectangular beam agree well with the "ten" rule of thumb. That is, if the aspect ratios of the structure are greater than ten, then the structure may be treated as a one dimensional Euler-Bernoulli beam.

The solid circular cylinder does not follow this rule of thumb. The aspect ratio approaches 50 before the one dimensional solution gives reasonable predictions. The errors for the lower aspect ratios of the cylinder were less than that for the same aspect ratios of the solid rectangular cross section. This is most likely due to the fact that the l/b ratio for the solid cylinder is larger than the l/b ratio for the

solid rectangular cross section at the lower aspect ratios. As the aspect ratio of the cylinder increases the decrease in error is not as great as in the rectangular cross section. This may indicate that circular cross sections need to be treated differently than rectangular cross sections.

The results for the square shell show similar trends as the solid cylinder. The square tested had very thin walls (.9 mm). This may account for the smaller errors at the lower aspect ratios. The one dimensional solution does not predict reasonable frequencies until the aspect ratio approaches 90.

The circular shell follows trends similar to the square shell. These structures are of the most interest because they are most like the composite structures tested. The one dimensional solution for the circular shell does not predict reasonable frequencies until the aspect ratio approaches 50 or 60. Rules of thumb for solid rectangular beams now no longer seem to apply to circular cross sections or thin shells. Based on these measurements and observations we would expect to see similar trends for the composite tubes.

The equation used to predict the frequencies of the composite tube was derived in the chapter describing the theoretical background and modified in the experimental procedures chapter. This equation is repeated below.

$$f_n = [(\beta_n l)^2/2\pi]\sqrt{(6R^2)/(h^3 \rho_0 d_{11}^* l^4)}$$

This equation was also applied to the aluminum circular shell as a check that it indeed reduces to the isotropic case. Table 12 shows the $\mathbf{Q}$ matrix symbolically for the aluminum. Also included in the table are the values of the $\mathbf{d}^*$ matrix, described earlier as the inverse of the bending stiffness matrix, calculated for the test specimen used. The value for Poisson's ratio used in the calculation was .25. Table 13 shows the predicted frequencies of the aluminum circular shell based on

the calculation of d_{11}^*. It can be seen from these results that the frequency equation used to calculate the frequencies of the composite tubes reduces to the prediction made for the isotropic case.

Table 14 shows the tests results for composite tube 1. Figure 29 is a bar chart of the percent error versus mode number for tube 1. Included in the table are a comparison of the predicted frequencies with those measured. The aspect ratio for this tube was 31. The results show that the frequency measured was very close to the frequency predicted. The error being less then 3 % for all the modes measured. We can not predict the effect of damping on the frequencies , but we would expect that damping would reduce the frequency. The negative percent error for modes two and three indicates that the measured frequency was higher than the predicted frequency. This may be because the specimen tested had longitudinal ridges running the length of the structure. The ridges were a result of the curing process and act as stiffeners. These stiffeners would make the fequencies of the structure higher.

Table 15 shows the test results for modes one, two and three for composite tube 2. Figure 30 is a bar chart of the percent error versus mode number for tube 2. The aspect ratio for this tube was 25. The test results show that the one dimensional solution for all three modes is in the neighborhood of 18 %. Table 16 shows the test results for modes four and five for composite tube 2. The error in the one dimensional solution for the fifth mode is also in the neighborhood of 18%. However, the error in the one dimensional solution for the fourth mode varies from near 10 % to as high as 22 %. The frequencies measured for the fourth mode for measurements two, four, and six were extracted using only one response coordinate (response location three or five). Frequencies for the fourth mode

could not be extracted from the other response coordinates. At these other locations the FRFs showed no distinct peak in the neighborhood of the predicted frequency. The frequencies extracted for modes one, two, three, and five were based on measurements from all six respose coordinates. This was also the case for composite tube 1.

Figures 31 and 32 present a comparison of the percent error in the first mode between the aluminum circular shell and the composite tubes. Figure 31 is for an l/d ratio of 25 (aluminum circular shell versus tube 2) and Figure 32 is for an l/d ratio of 31 (aluminum circular shell versus tube 1).

C. DISCUSSION

Studying the results for the tests on the aluminum structures indicates that the one dimensional solution to the frequency of vibration is an acceptable simplification if the aspect ratios approach 50. The aspect ratios of the composite tubes were 31 and 25 respectively. Based on these numbers alone we would not expect the one dimensional solution to predict the natural frequencies well. This was not the case. For composite tube 1 the one dimensional solution predicted the frequencies quite well. For composite tube 2 the one dimensional solution predicted the frequencies with quite a large error. We can compare directly the aspect ratio for the composite tubes and the aluminum tube. For an aspect ratio of 25 the aluminum tube had an error of 12 %. The composite tube with an aspect ratio of 25 had an average error of 18 %. This difference in perecentage error is reasonable because the composite structure is very complex. In the composite structure there is bending-twisting coupling, bending-extension coupling, and interaction between the ply layers. For the aluminum structure there are none of these complicating factors. We would therefore expect the error in the composite

tube to be larger than in the aluminum tube. For an aspect ratio of 30 the aluminum had an error of 10 %. The composite tube with an aspect ratio of 31 had an error of 2 %. This does not fit the pattern established by the aluminum test structures and followed by composite tube 2. The error found in the composite tube may improve quicker as the aspect ratio increases because the ratio of the in plane modulus to the transverse modulus is much larger for the composite than the aluminum. This effect should be further investigated as the aspect ratio increases. More tests on similar structures should be done to compare to the results from this test.

As the mode number increased in tube 2, the average error decreased. This is because as the mode number increased the displacements due to these modes decreased. Therefore, there was less out of plane displacement due to these modes. However, as the mode number increases a point would be reached where the distances between nodes were small enough that shear deformation effects would be significant. This would increase the error of the one dimensional prediction.

The difficulties encountered in extracting the fourth frequency in the second composite tube is due to the location of the response coordinates. The response coordinates were near the location of nodes of the fourth mode and near locations of anti nodes for the third and fifth modes. This would account for the lack of a distinct peak at the predicted frequency of the fourth mode.

Figures 33 through 38 are samples of the measured mode shapes and the predicted mode shapes for modes one, two and three. These mode shapes were from composite tube 2. This tube had an average error of 18 % in predicting the frequencies. Examination of the measured mode shapes indicates that the shapes

are very close to those predicted. The location of the nodes for the measured modes shapes are in error by approxiamately 10 %. These figures indicate that the shape of the displacement of the composite tube follows very closely to the one dimensional solution. For larger aspect ratios this error may decrease similarly to the prediction for the frequency.

Figure 39 is a representative example of the FRFs measured in this work. Figure 40 is the circle fit of the FRF data in Figure 39. To execute a circle fit, data fit bands were defined about the peaks of the FRF. The size and location of the fit was dependent upon the sharpness of the peak. If the peak was symmetric about the maximum value, then the fit band was symmetric about this frequency. For peaks of this type the fit bands were three to five spectral lines to each side of the maximum value. If the peak was skewed, then the fit band was also skewed. If the peaked was skewed to the left, the right side of the peak would be very steep (have a very large negative slope). On this side of the peak the fit band limit was three to five spectral lines from the maximum value. On the skewed side of the of the maximum value the fit band limit was five to fifteen spectral lines from the maximum value. For peaks skewed to the right, the fit band limits were reversed. For peaks which were not sharp, the fit band limits were placed five to fifteen spectral lines from the maximum. Within the limits of the fit bands the real and imaginary parts of the FRF were circle fit using a least squares method. The resulting plot is the familiar Nyquist plot. From this fit the frequencies and damping were found.

V. SUMMARY AND CONCLUSIONS

The results of this investigation are summarized below.

1. The factors which determine whether a structure may be treated as a one dimensional Euler-Bernoulli beam are the length to depth ratio and the length to width ratio. Both of these ratios must be larger than ten in order to treat a solid rectangualar cross section as a one dimensional problem.

2. When the cross section is no longer rectangular the aspect ratios must be larger than ten in order to treat the structure one dimensionally. For solid circular cross sections these ratios may need to approach 50. For shell structures these aspect ratios may need to vary from 50 to 100.

3. The treatment of a composite shell as a one dimensional structure is dependent on the aspect ratios. For composite shells aspect ratios may need to approach 50 before the one dimensional solution gives reasonable solutions.

Further study should continue using the Euler-Bernoulli model. Testing should be done on structures with various aspect ratios. Tests should also be done on structures of diffeerent cross sections. Included should be tests on elliptic, rectangular, and other useful cross sections. Laminates of greater thickness should be investigated in order to determine when the thickness becomes to great for this model to predict accurately the natural frequencies and mode shapes. The addition of shear deformation effects should be investigated to improve the model. Testing done in this work was of relatively easy laminate stacking sequences. The effect of unsymmetric laminate stacking sequence should be investigated. This is important because then the **A, B,** and **D** matrices do not have any zero value

elements. This may violate the assumption that the displacements due to Poisson's ratio terms are negligible. The laminated shell theory equations should be investigated for further simplification. This may result in a simplified treatment more accurate then the present model.

The unique properties of composite materials allows the designer to tailor the material to his needs. This is done by determing the optimal angle orientation of the fiber. For complex structures the designer must turn to Finite Element Methods and the computer for computational power. In doing so, the designer may lose their "feel" for the structure they are designing. What has been presented in this work is a tool, when used within the limits of its approximations, which allows the designer to keep their heuristcal "feel" to design . The results presented provide for timely computation and sufficient accuracy for "back of the envelope" calculations.

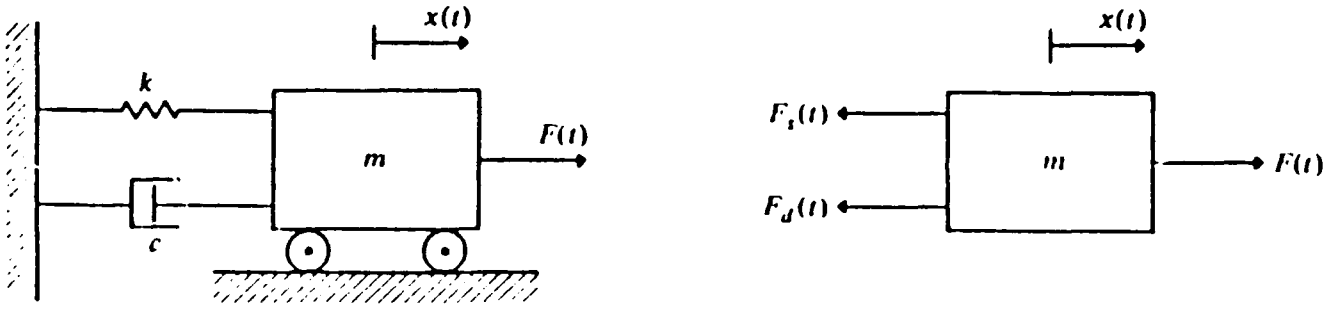

Figure 1. Mass, damper, and spring system with free body diagram [Ref. 13]

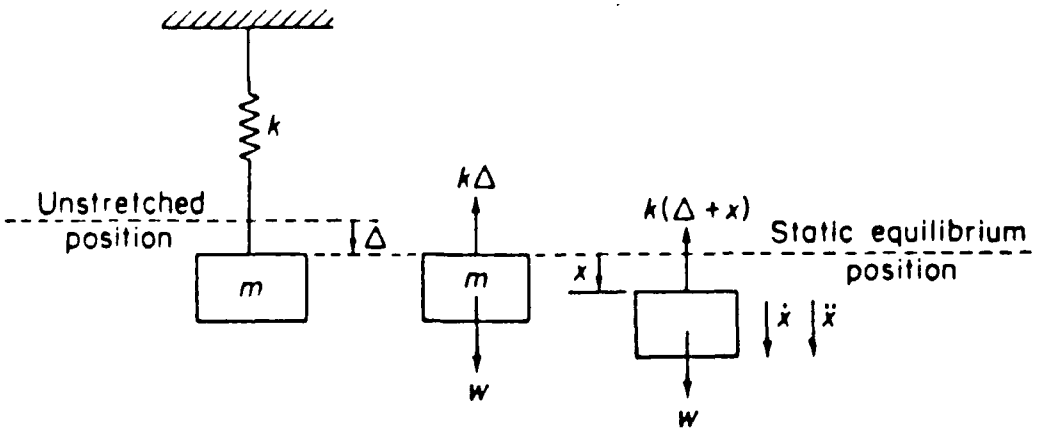

Figure 2. Undamped mass- spring system with free body diagram [Ref. 14]

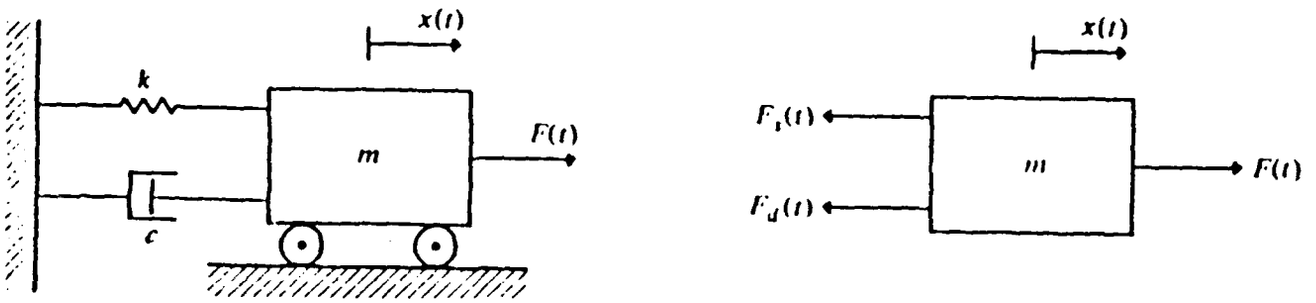

Figure 3. Damped mass-spring system with free body diagram [Ref. 13]

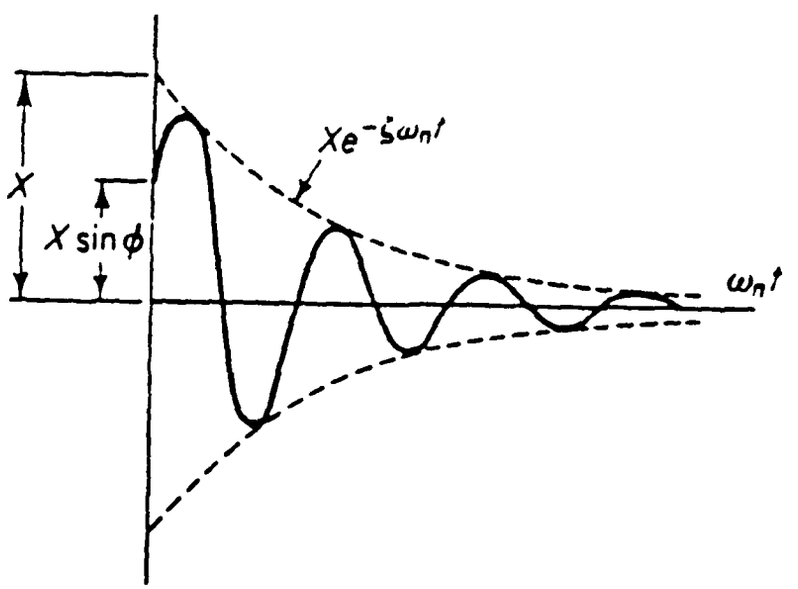

Figure 4. Underdamped motion - $\zeta < 1$ [Ref. 14]

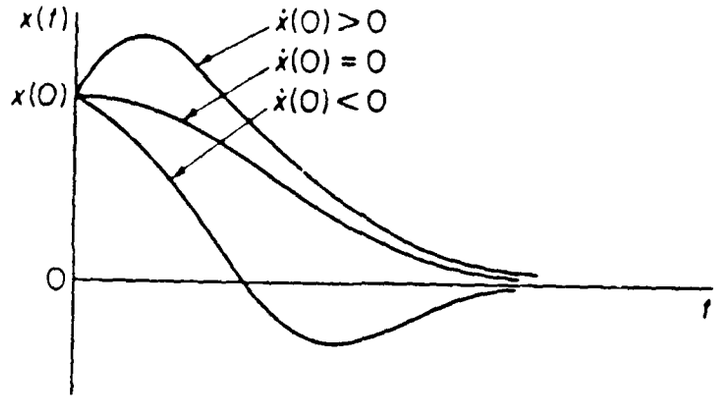

Figure 5. Critically damped motion for various initial velocities - $\zeta = 1$ [Ref. 14]

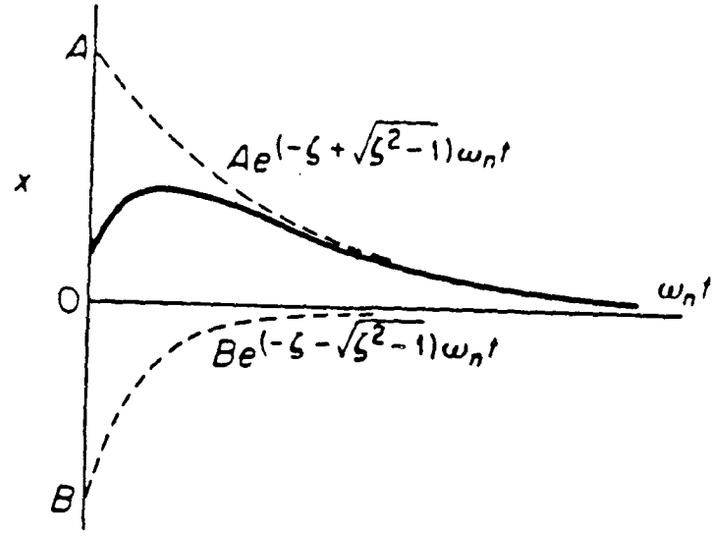

Figure 6. Overdamped motion - $\zeta > 1$ [Ref. 14]

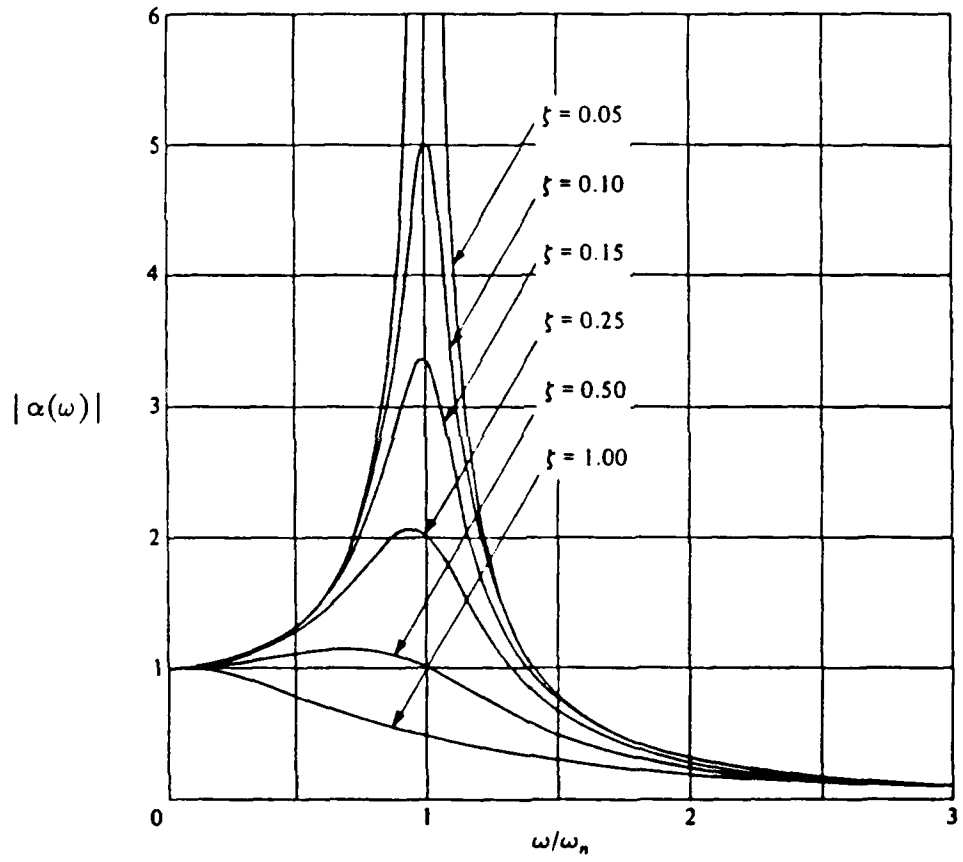

Figure 7. $|\alpha(\omega)|$ vs ω/ω_n [Ref. 13]

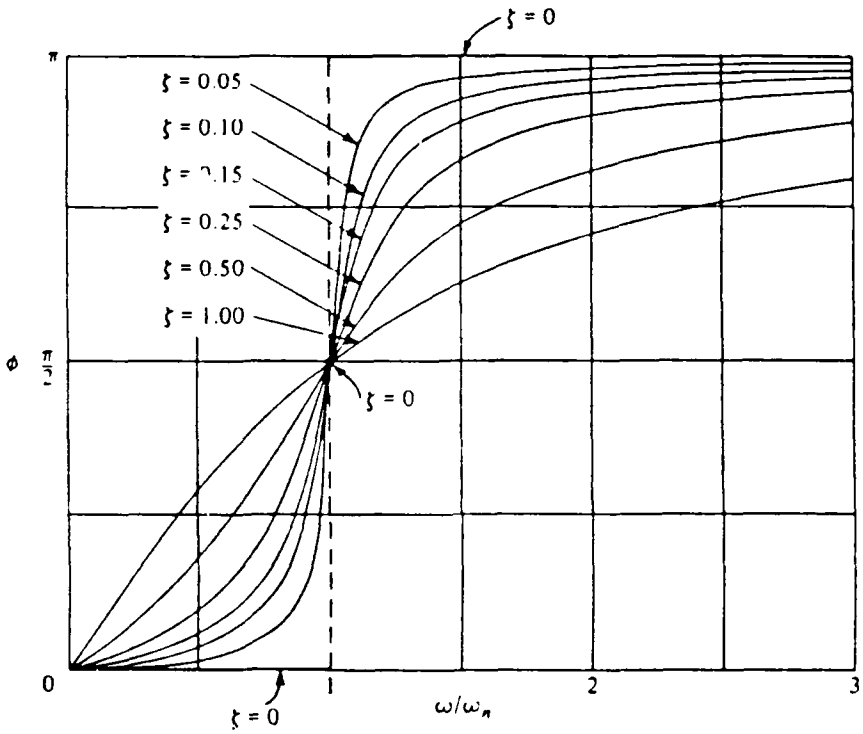

Figure 8. ϕ vs ω/ω_n [Ref. 13]

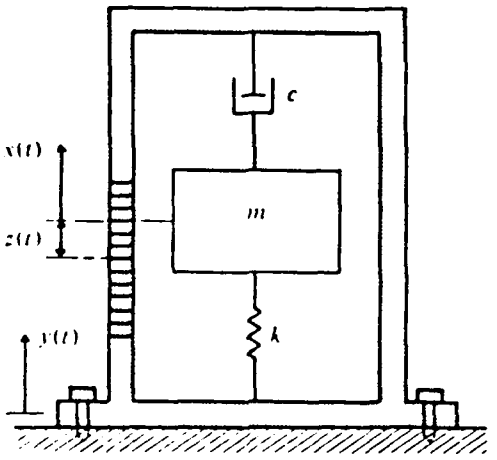

Figure 9. SDOF model of accelerometer [Ref. 13]

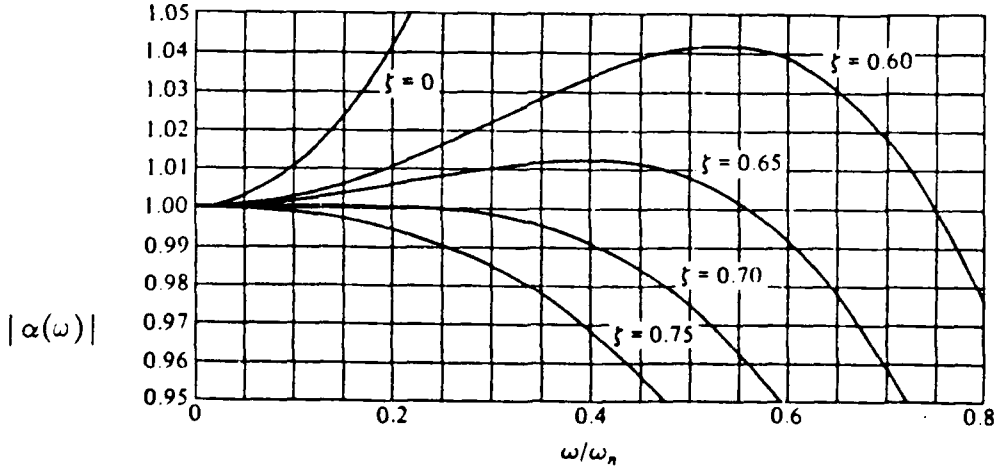

Figure 10. $|\alpha(\omega)|$ vs ω/ω_n for accelerometer [Ref. 13]

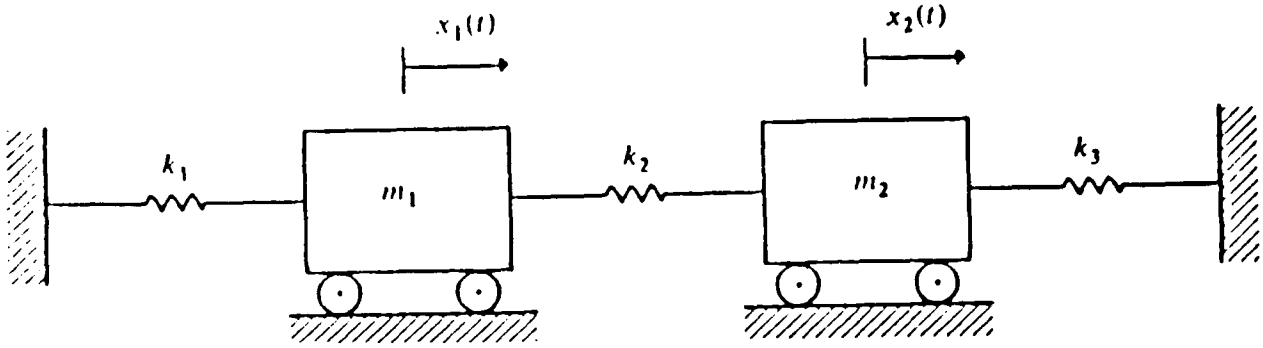

Figure 11. Two degree of freedom undamped system [Ref. 13]

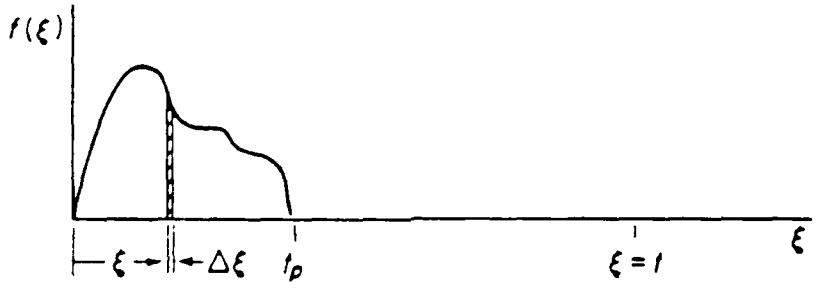

Figure 12. Force impulse [Ref. 14]

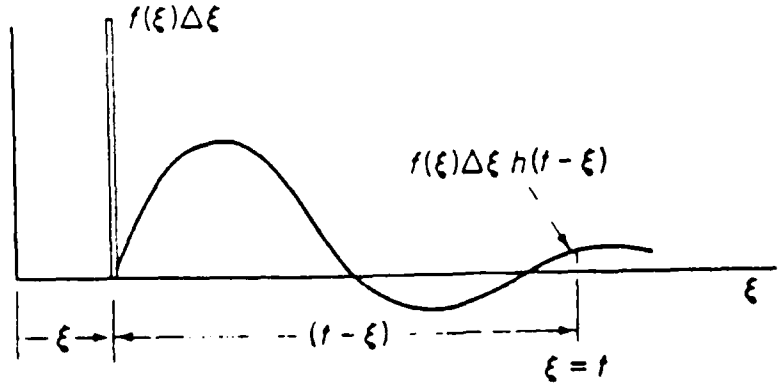

Figure 13. Force impulse response [Ref. 14]

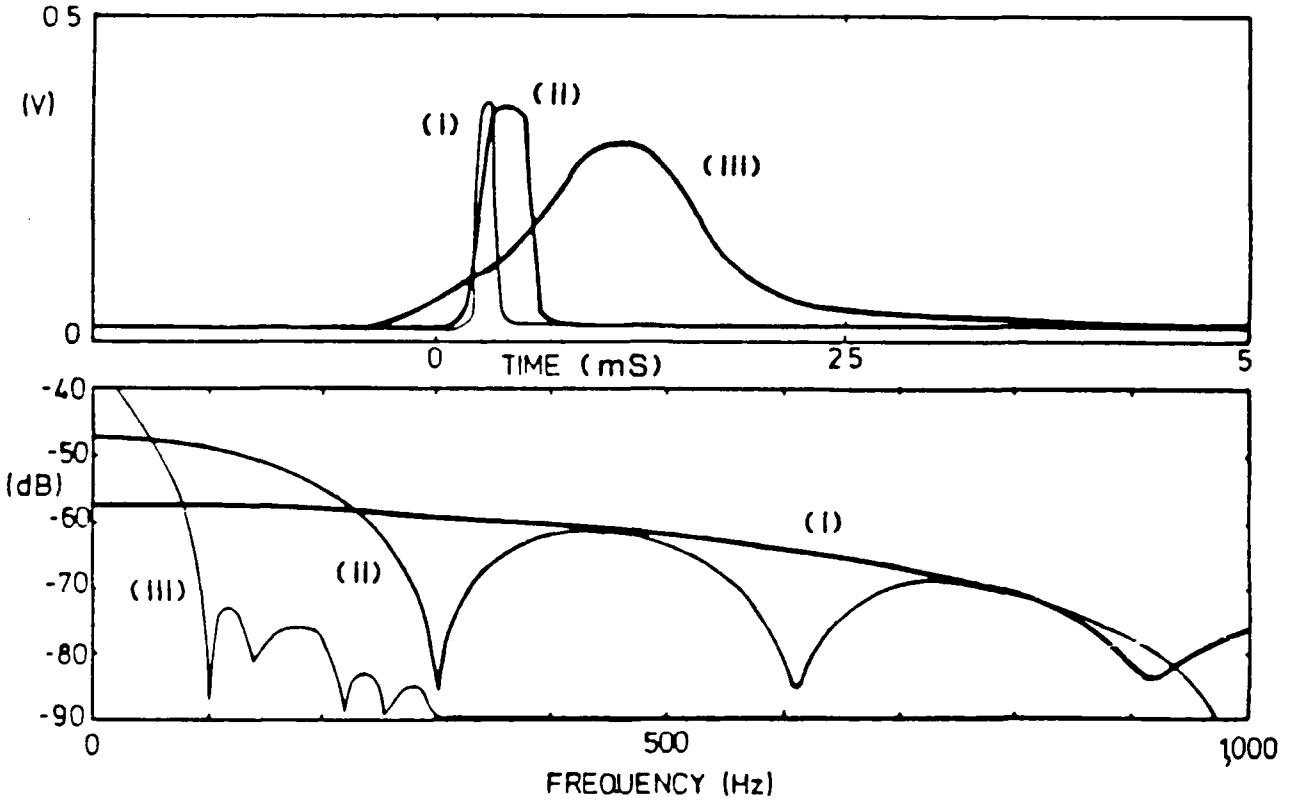

Figure 14. Force impulses and spectra [Ref. 22]

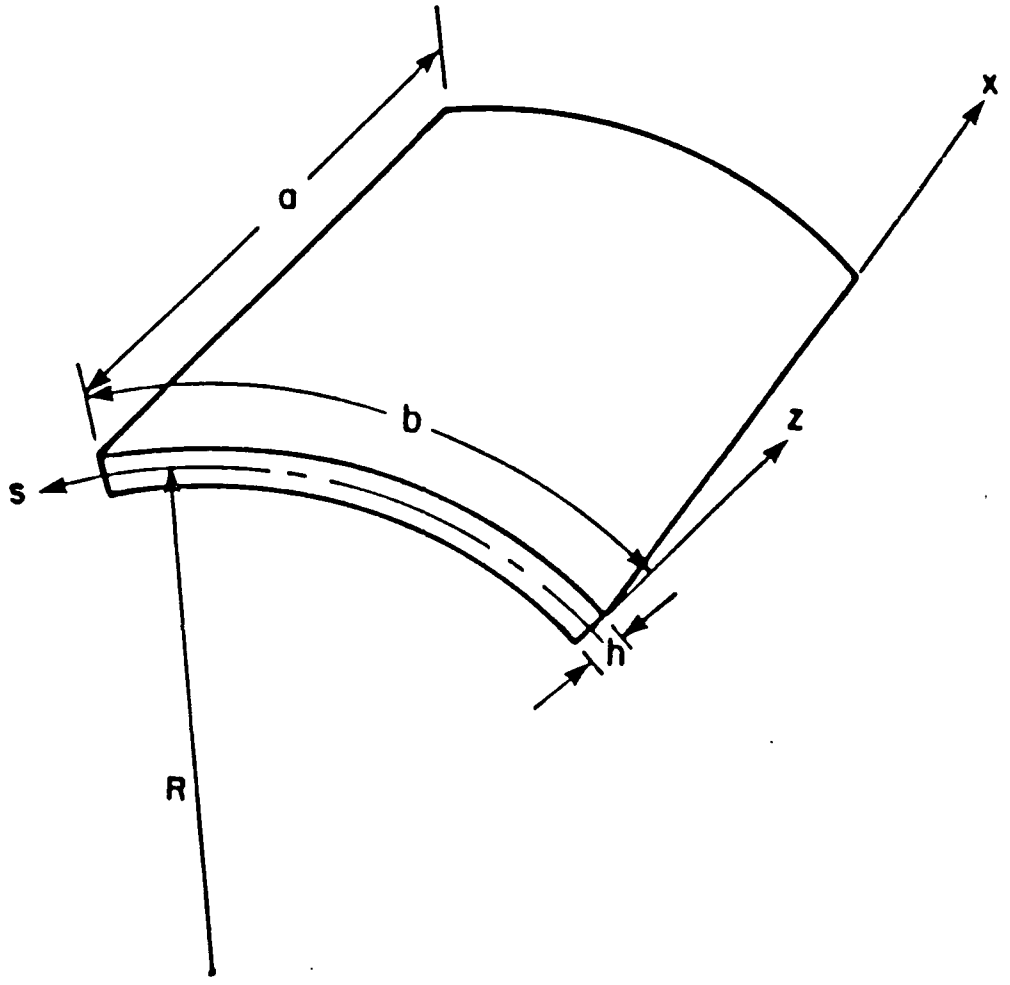

Figure 15. Reference coordinate system [Ref. 15]

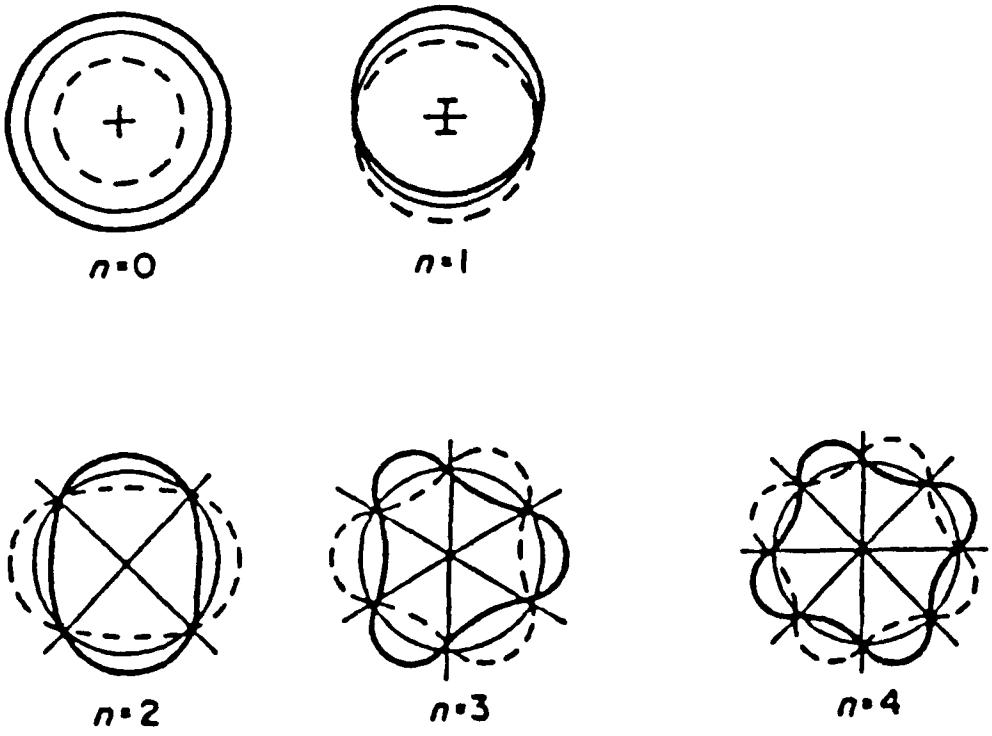

Figure 16. Circumferential modes of vibration [Ref. 7]

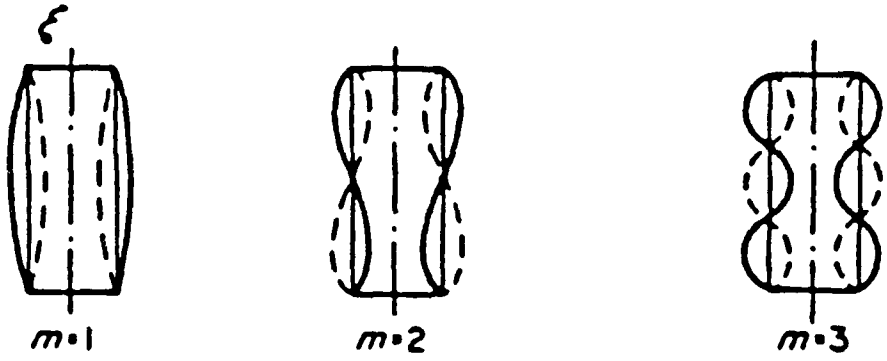

Figure 17. Axial modes of vibration [Ref. 7]

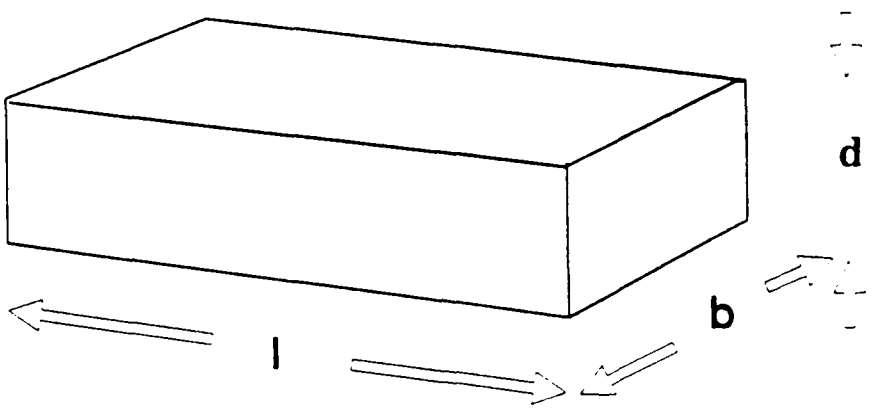

Figure 18. Aluminum test piece - rectangular cross section

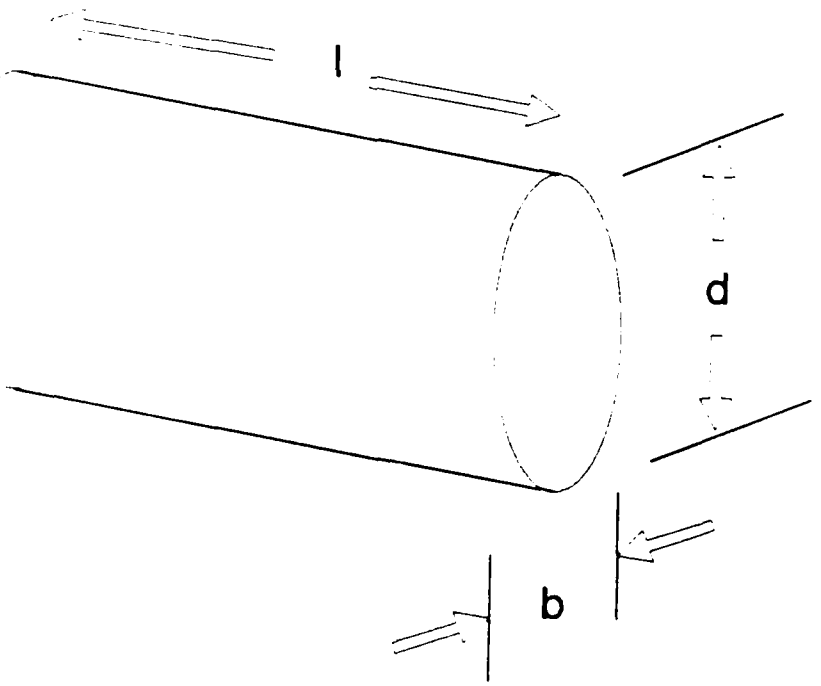

Figure 19. Aluminum test piece - circular cross section

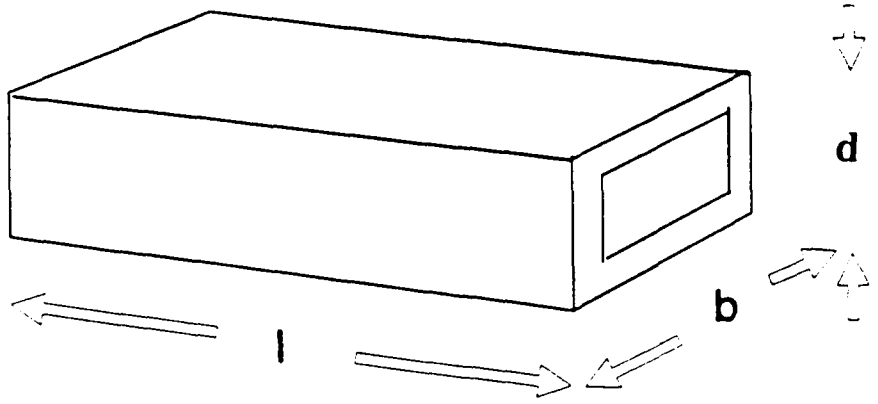

Figure 20. Aluminum test piece - box shell

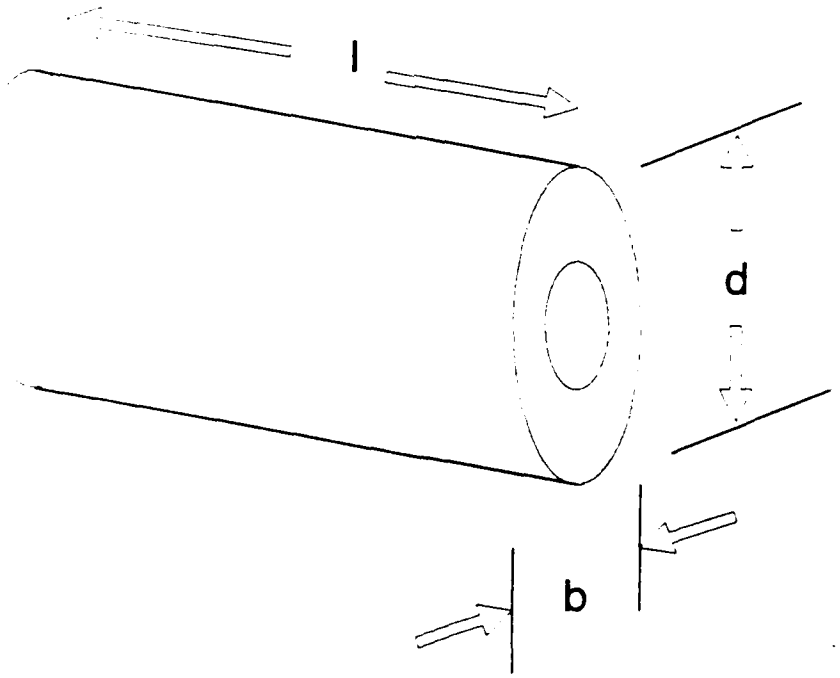

Figure 21. Aluminum test piece - circular shell

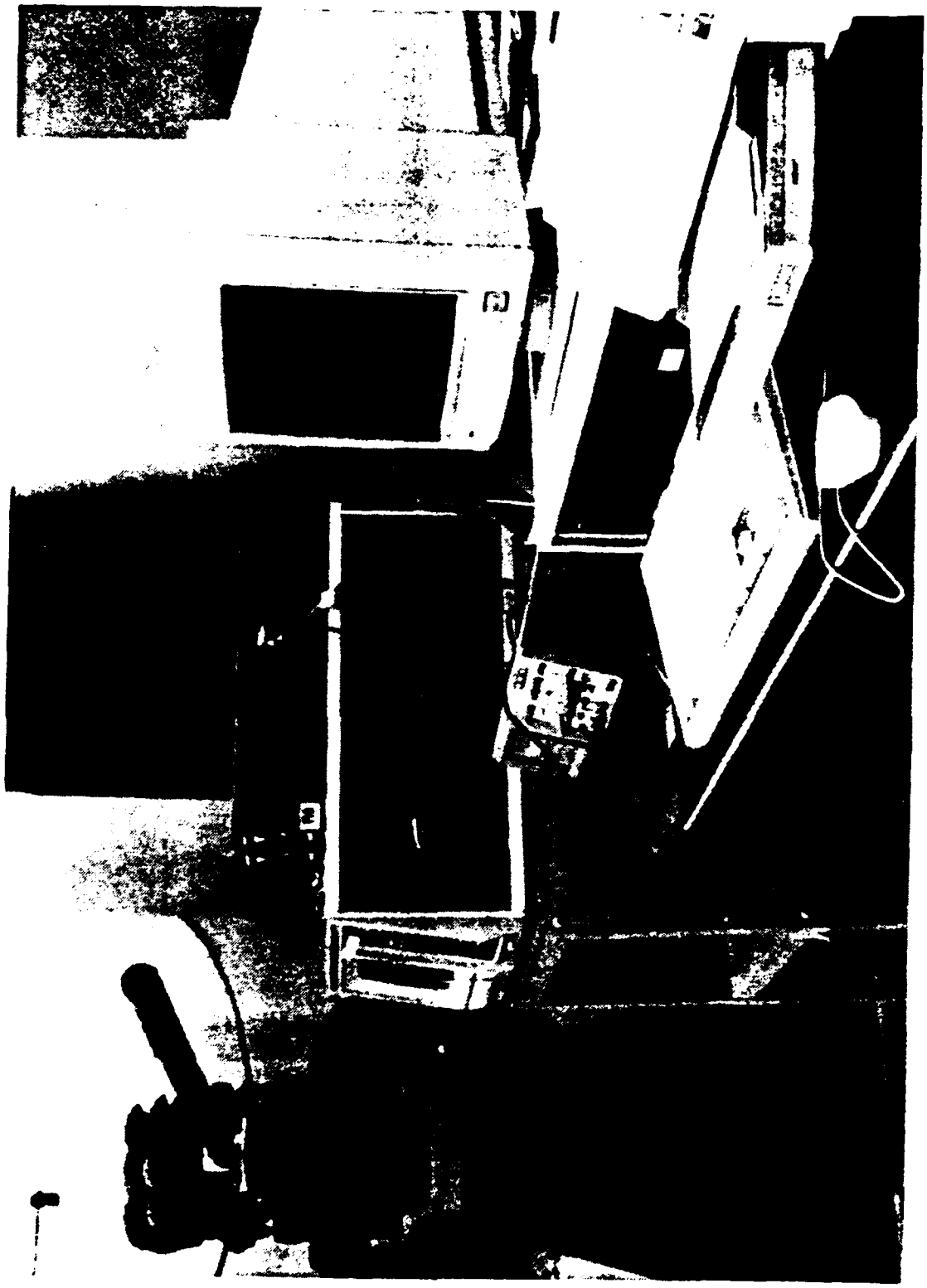

Figure 22. Photograph of test area

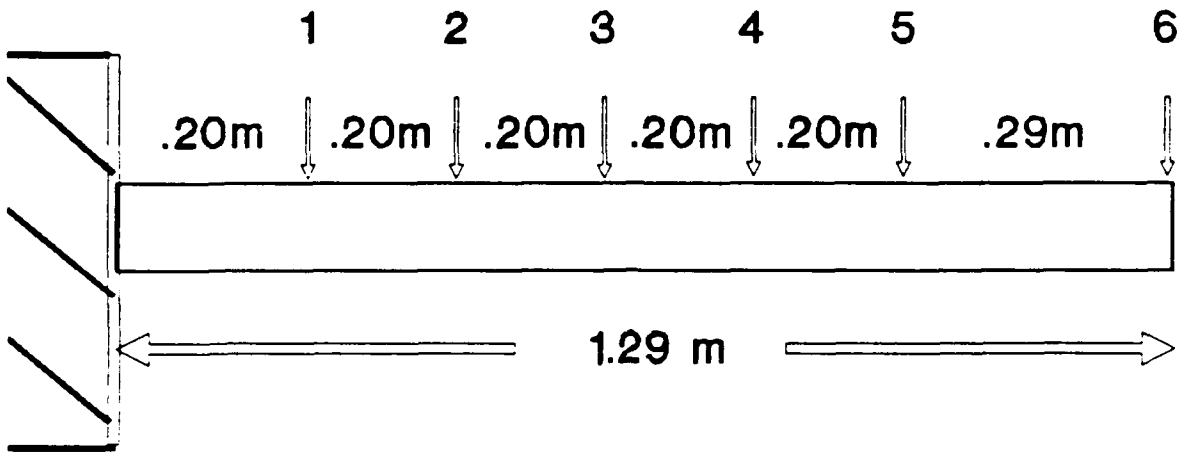

Figure 23. Degrees of Freedom/Response Coordinate locations - Tube 1

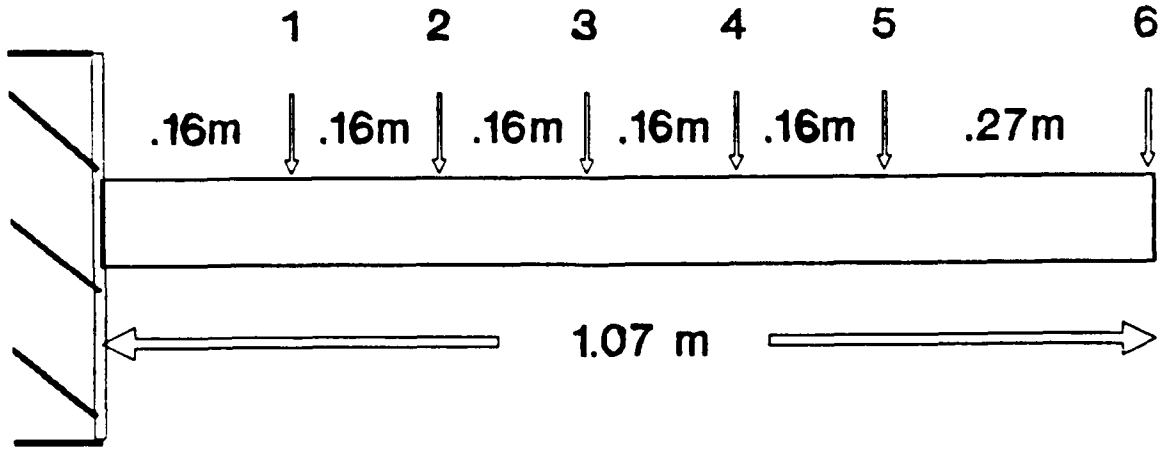

Figure 24. Degrees of Freedom/Response Coordinate locations - Tube 2

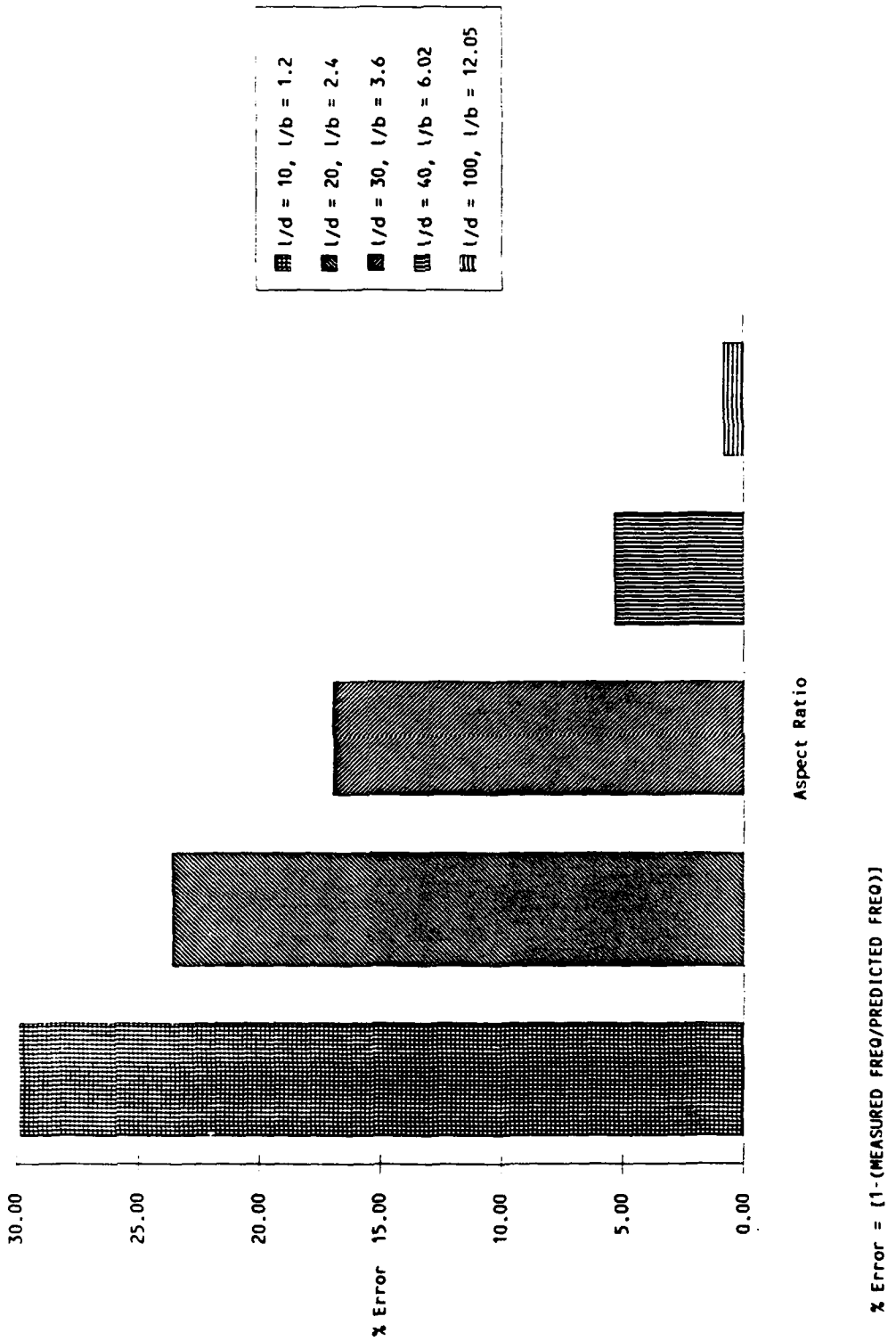

Figure 25. Percent Error vs Aspect Ratio - Aluminum Rectangular Cross Section

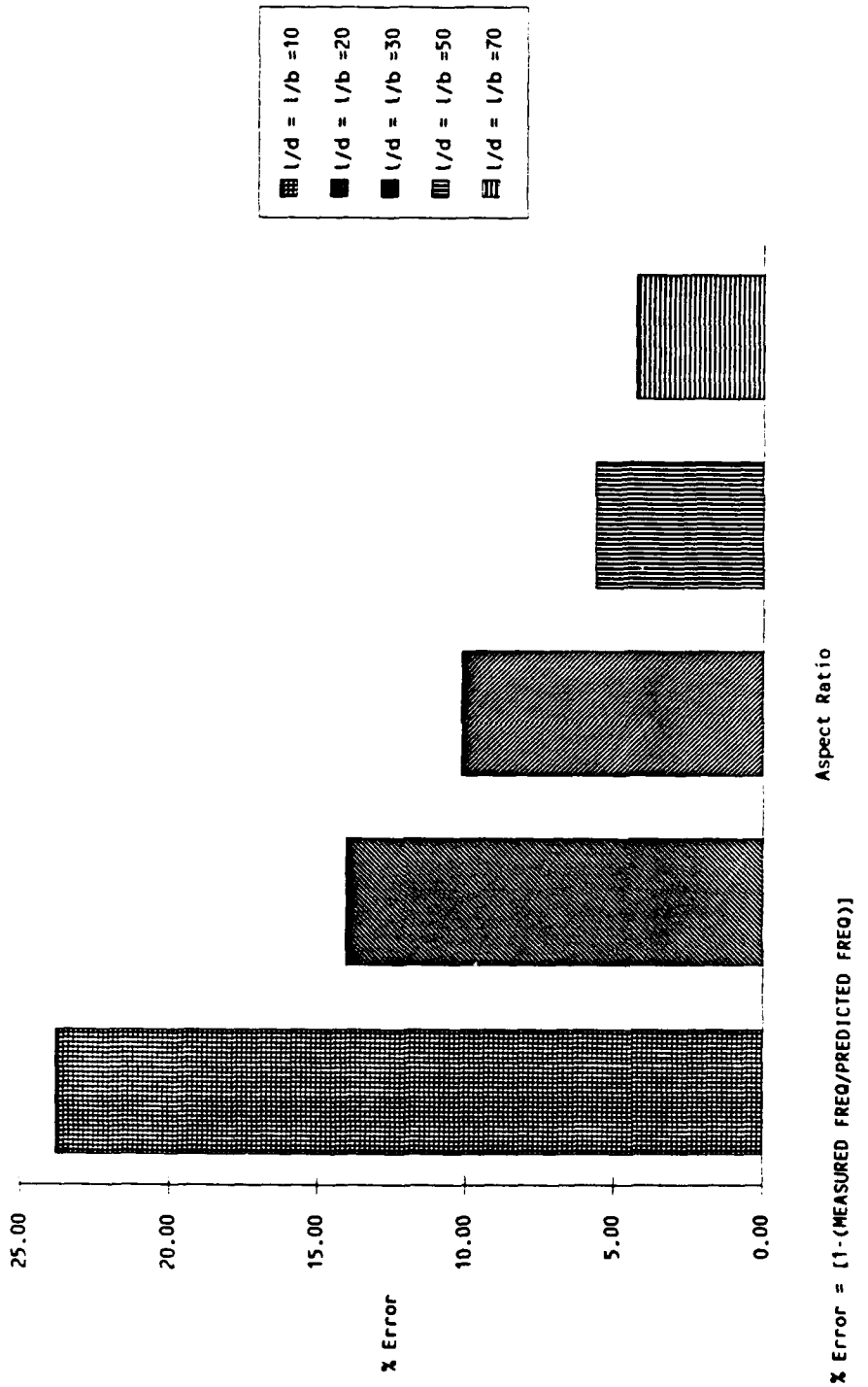

Figure 26. Percent Error vs Aspect Ratio - Aluminum Solid Cylinder

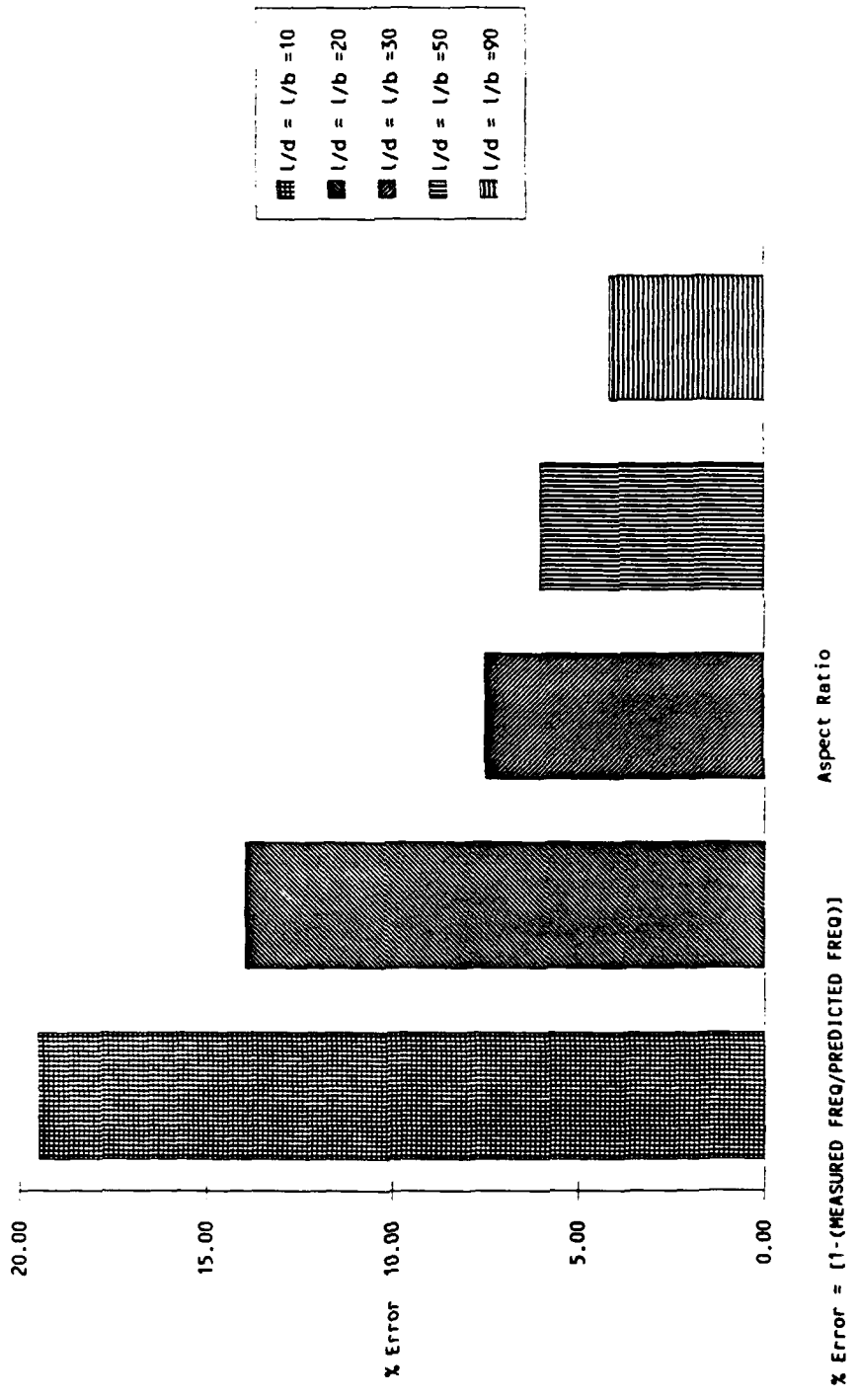

Figure 27. Percent Error vs Aspect Ratio - Aluminum Square Shell

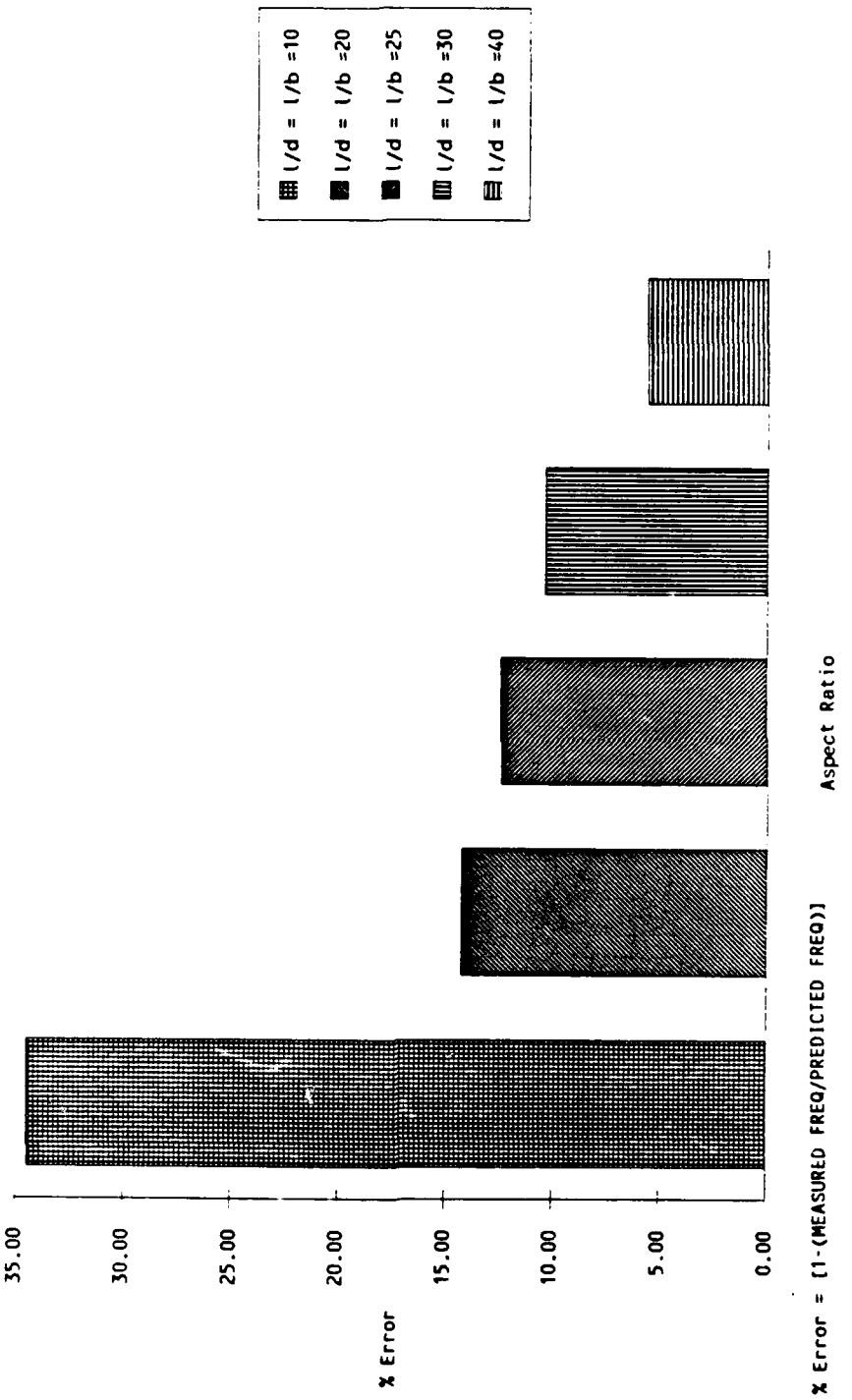

Figure 28. Percent Error vs Aspect Ratio - Aluminum Circular Shell

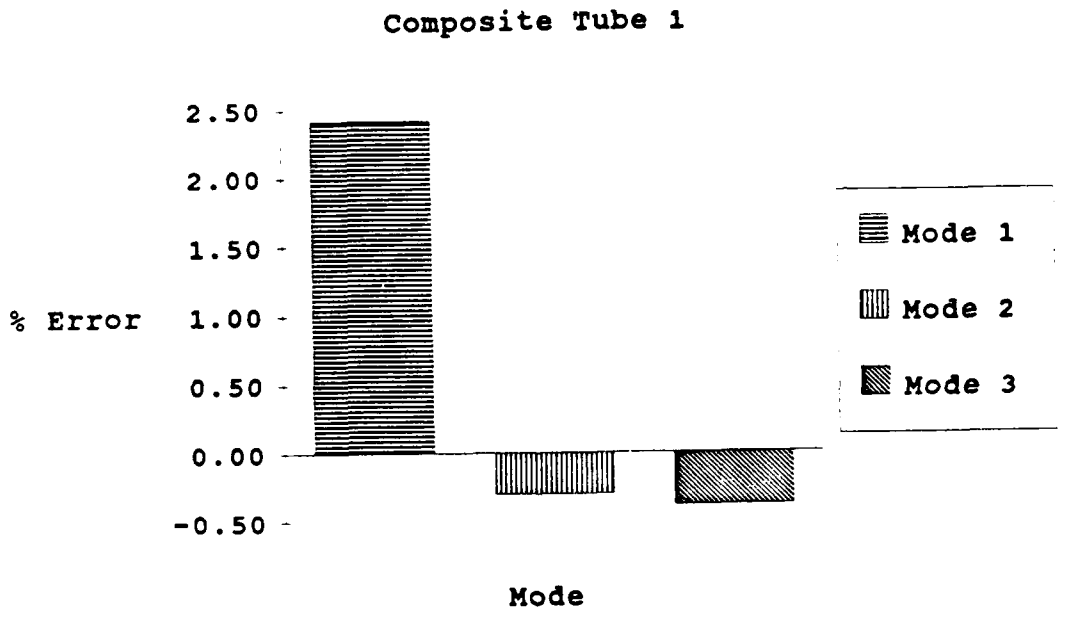

Figure 29. Percent Error vs Mode - Composite Tube 1, l/d = 31

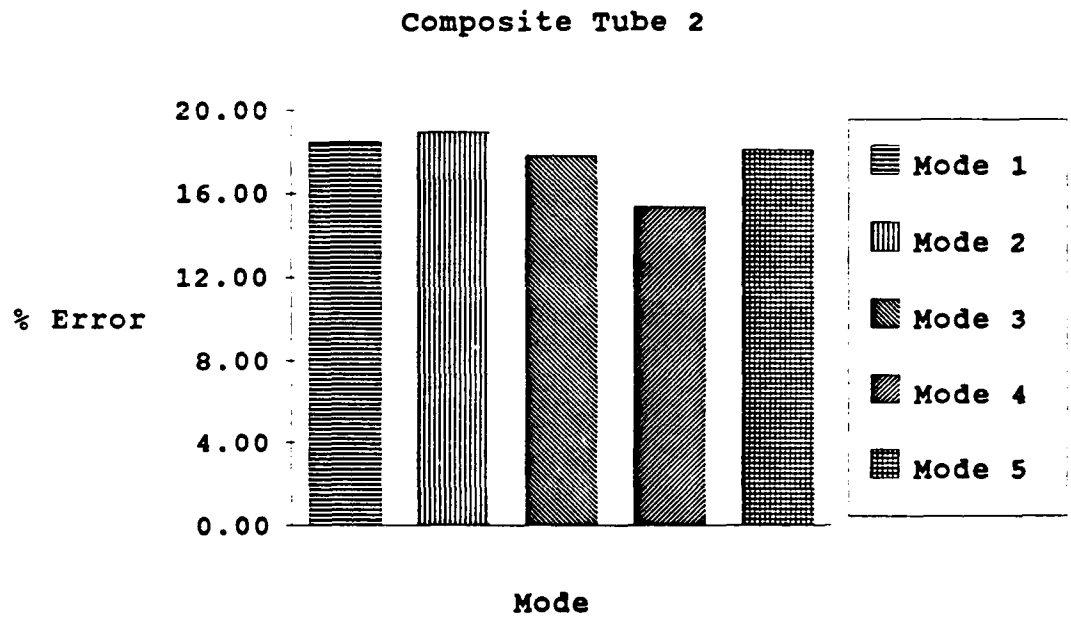

% Error = [1-(MEASURED FREQ/PREDICTED FREQ)]

Figure 30. Percent Error vs Mode - Composite Tube 2, l/d = 25

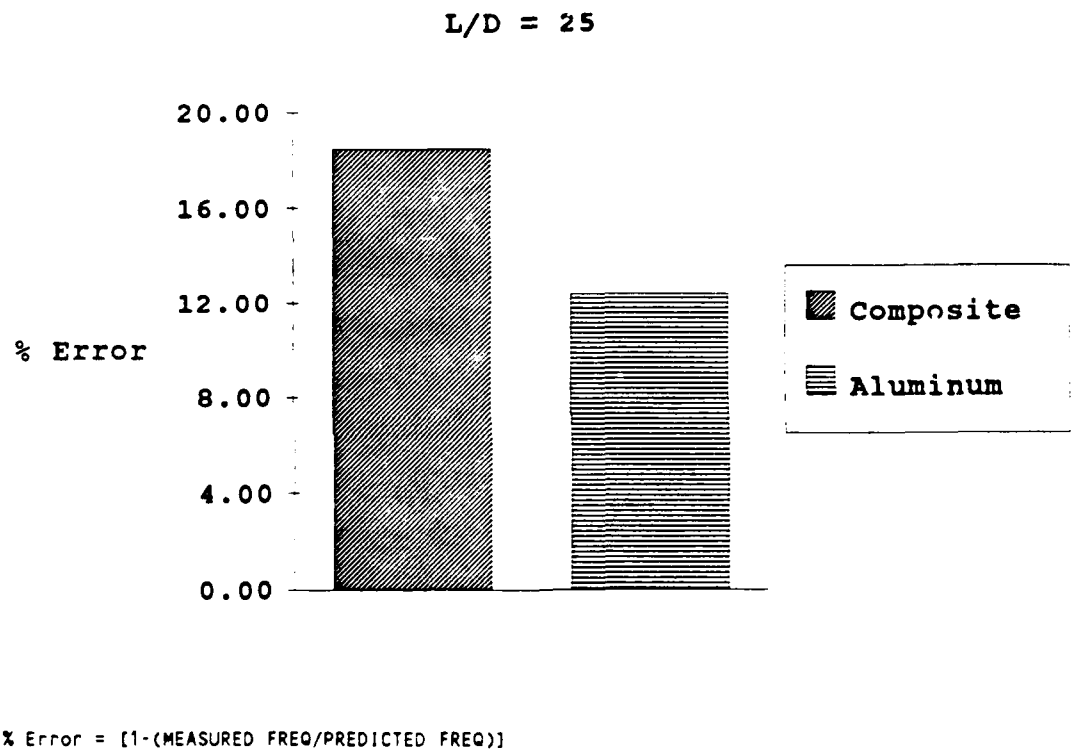

Figure 31. Comparison of Percent Error in Mode 1 between Aluminum Circular Shell and Composite Tube for l/d = 25

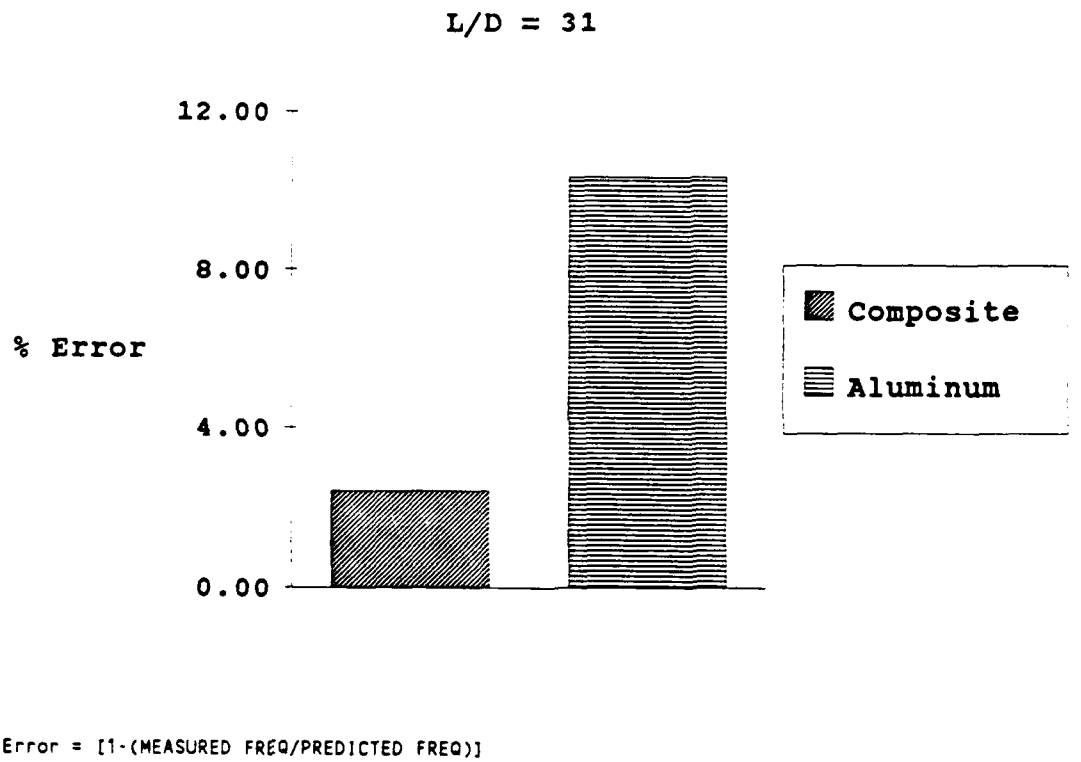

Figure 32. Comparison of Percent Error in Mode 1 between Aluminum Circular Shell and Composite Tube for l/d = 31

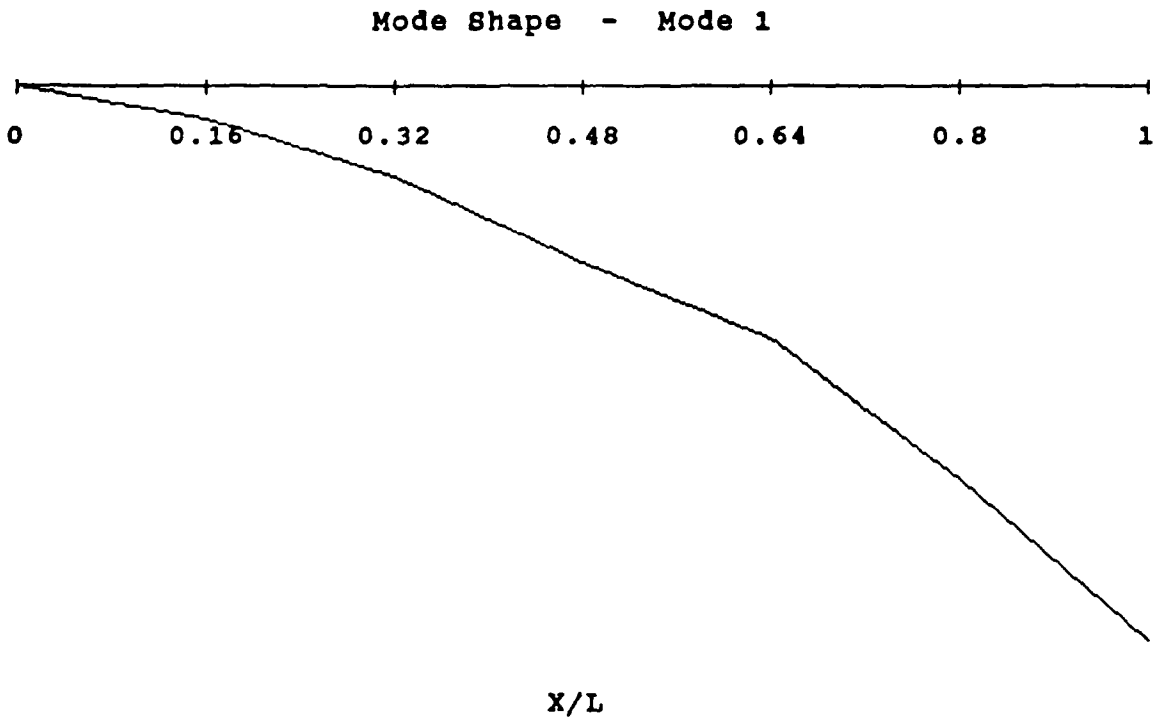

Figure 33. Measured mode shape 1

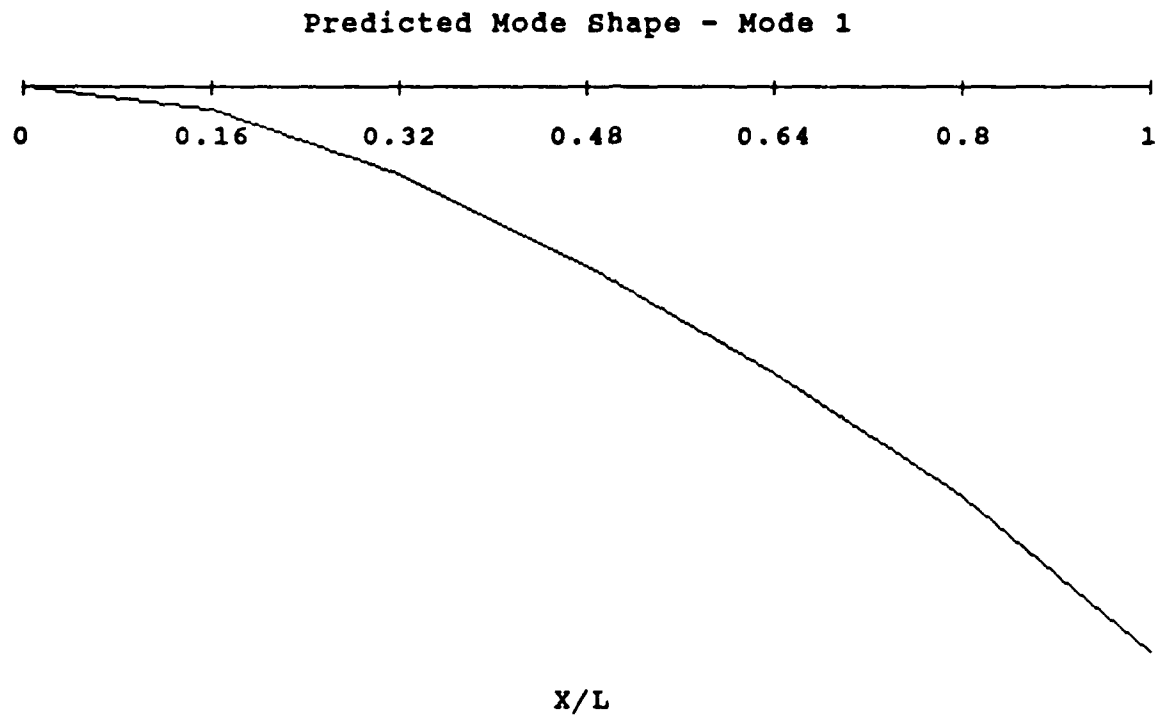

Figure 34. Predicted mode shape 1

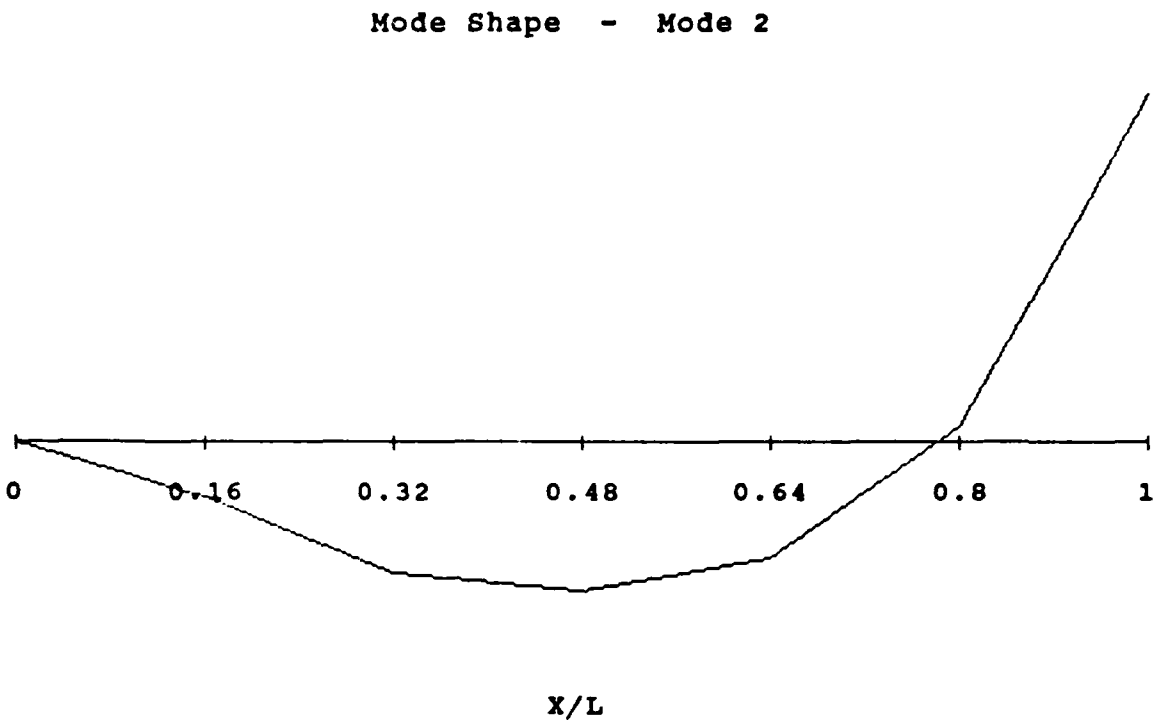

Figure 35. Measured mode shape 2

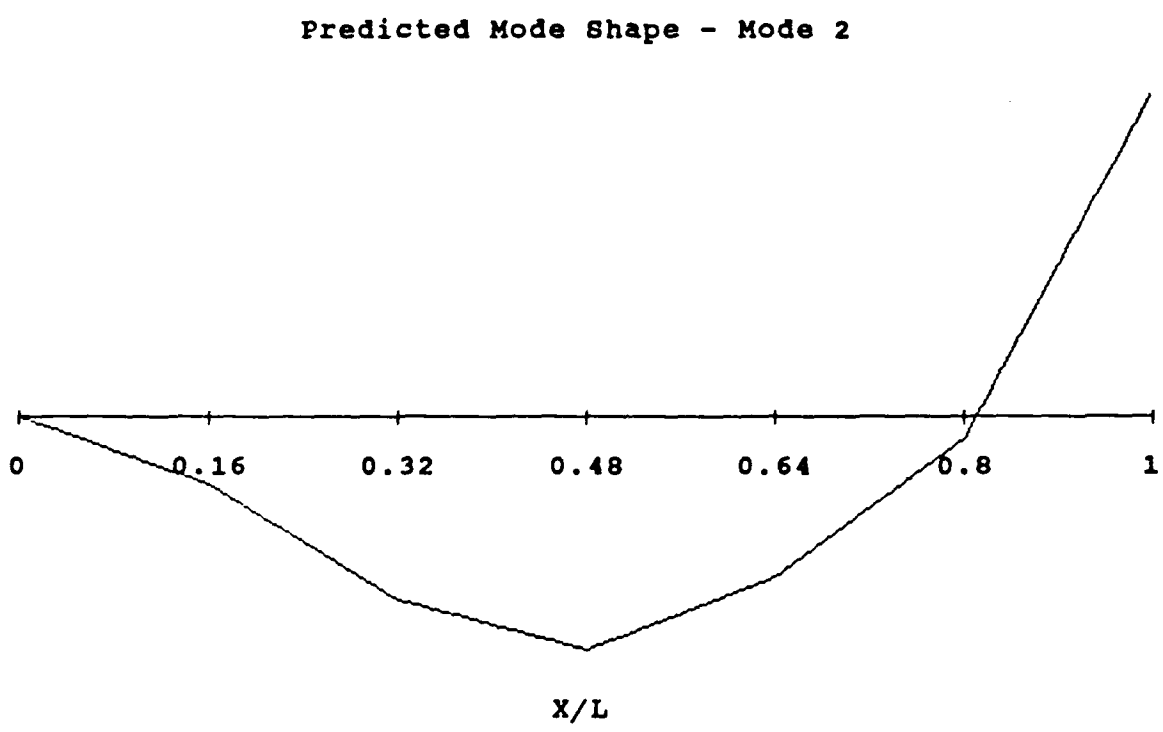

Figure 36. Predicted mode shape 2

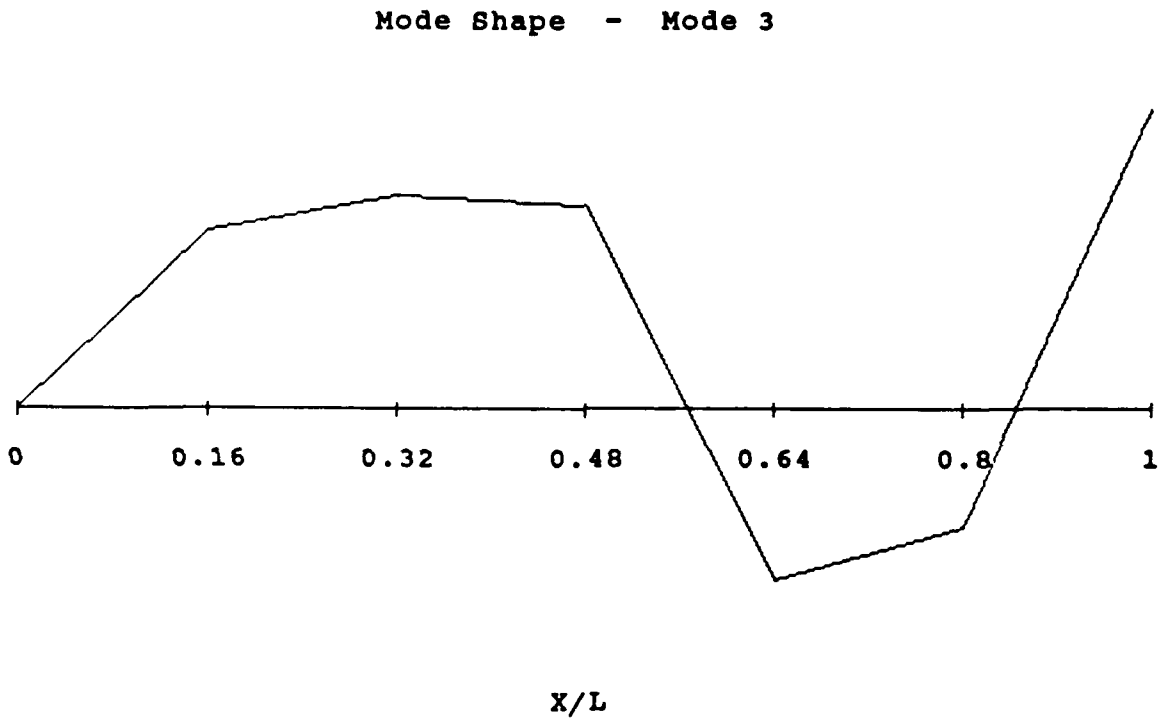

Figure 37. Measured Mode Shape 3

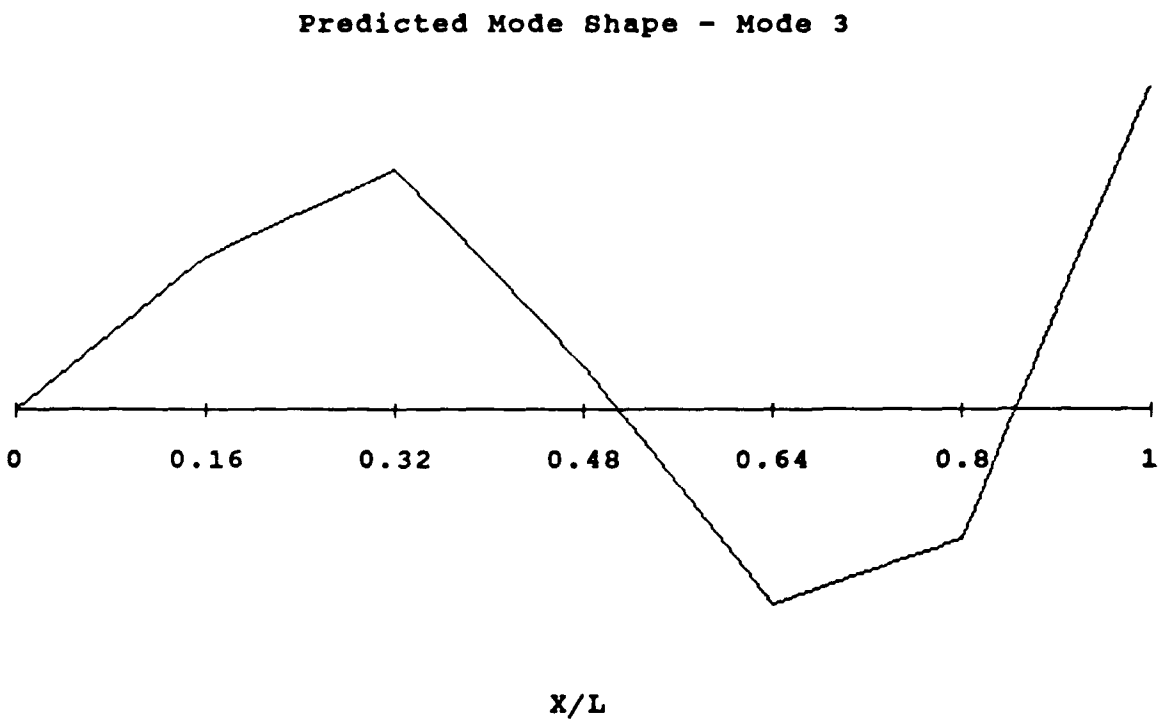

Figure 38. Predicted Mode Shape 3

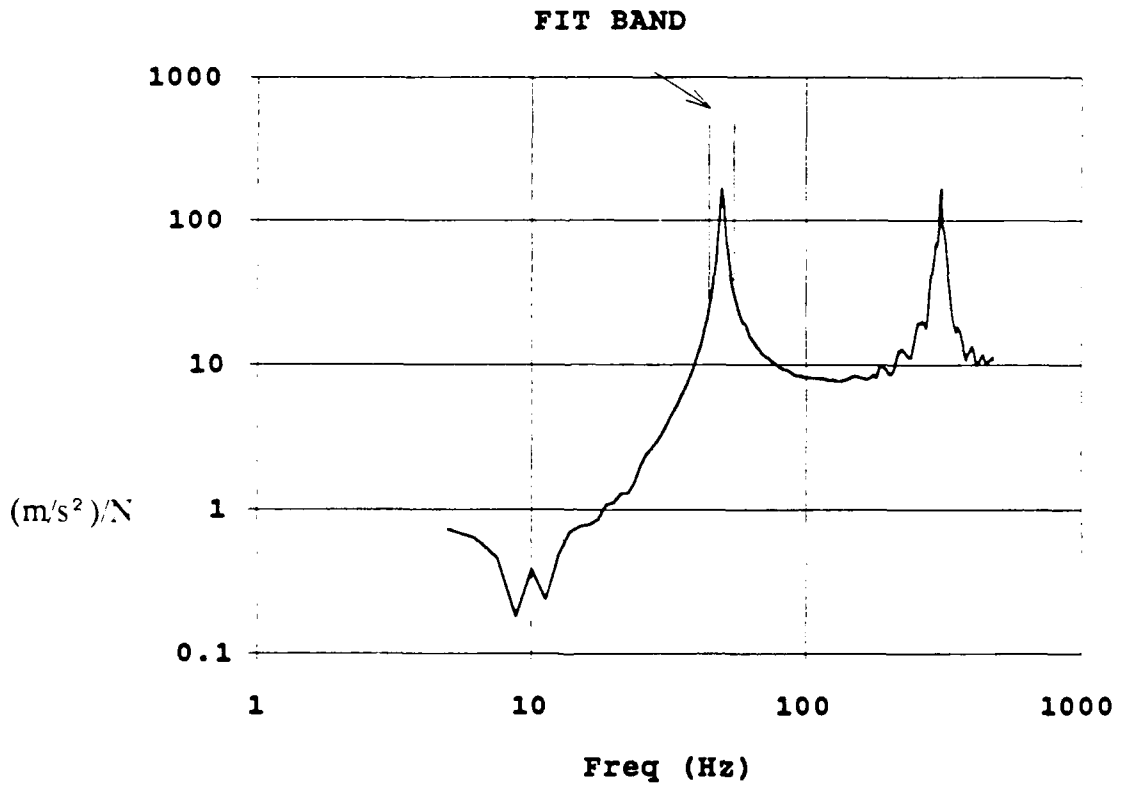

Figure 39. FRF plot for Aluminum Beam

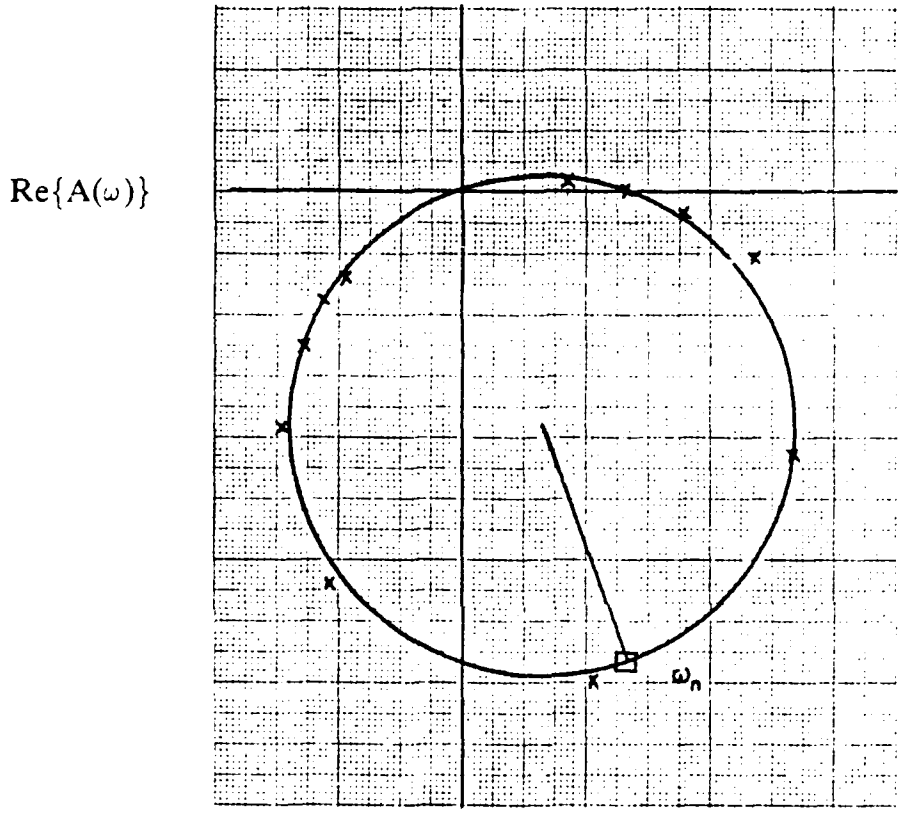

Figure 40. Circle fit of FRF data

TABLE 1. DESCRIPTION OF ALUMINUM TEST SPECIMEN

GEOMETRY	I (m^4)	A (m^2)	l/d	l (m)
Rectangle	1.12E-09	0.000335	10	0.064
			20	0.127
			30	0.191
			50	0.318
			100	0.635
Solid Cylinder	6.46E-09	0.000285	10	0.191
			20	0.381
			30	0.572
			50	0.953
			70	1.334
Square Shell	3.56E-09	0.0000646	10	0.191
			20	0.381
			30	0.572
			50	0.953
			90	1.715
Circular Shell	1.03E-08	0.0000863	10	0.318
			20	0.635
			25	0.794
			30	0.953
			40	1.270

TABLE 2. MATERIAL PROPERTIES AND LINEAR COMBINATIONS

Type	CFRP
Fiber	AS-4
Matrix	976 Epoxy
Engineering constants ,GPa	
Ex	138.00
Ey	8.96
nu/x	0.30
Es	7.10
V/f	0.66
rho	1.60
ho,mm	0.125
Ply stiffness, GPa	
Qxx	138.81
Qyy	9.01
Qxy	2.70
Qss	7.10
Linear Combinations,GPa	
U1	59.66
U2	64.90
U3	14.25
U4	16.95
U5	21.35

AD-A219 227 TRANSVERSE VIBRATIONS OF A COMPOSITE CYLINDRICAL TUBE OF CIRCULAR CROSS SECTION(U) NAVAL POSTGRADUATE SCHOOL MONTEREY CA R W ETTER SEP 89

UNCLASSIFIED F/G 22/2 NL

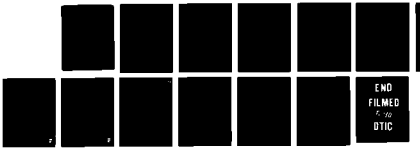

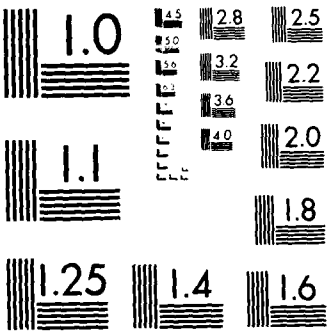

TABLE 3. GEOMETRY AND LAYUP - TUBE 1

Length(m)	1.292
OD (m)	0.0417
ID (m)	0.0376
R (m)	0.0198
L/D	31
h (m)	0.00205
I (m^4)	5.03E-08
A (m^2)	0.000255

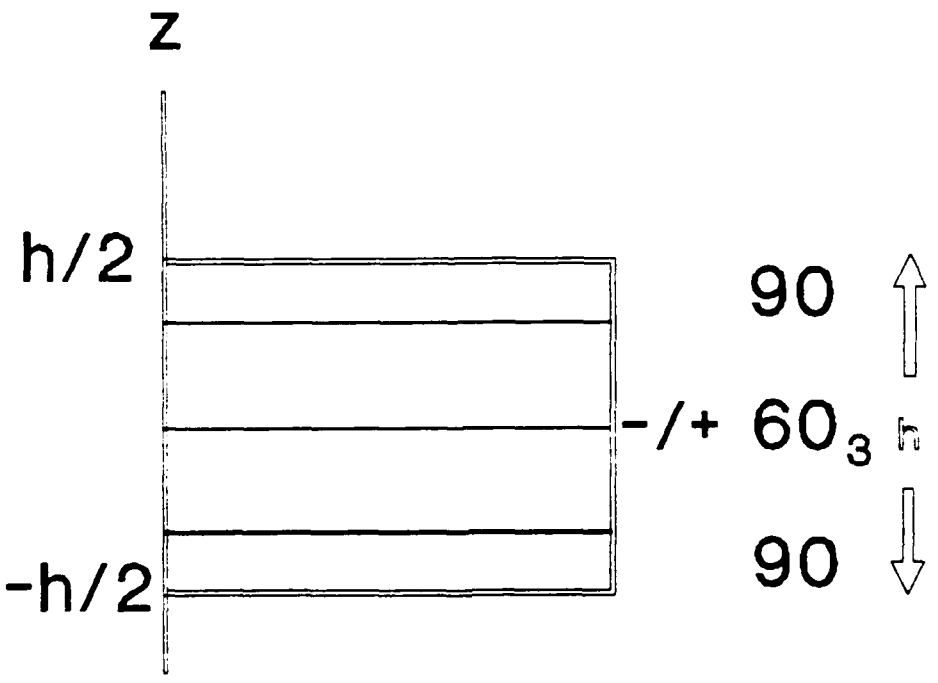

TABLE 4. GEOMETRY AND LAYUP - TUBE 2

Length(m)	1.07
OD (m)	0.0427
ID (m)	0.0381
R	0.0202
L/D	25
h (m)	0.00229
I (m^4)	5.93E-08
A (m^2)	0.00029

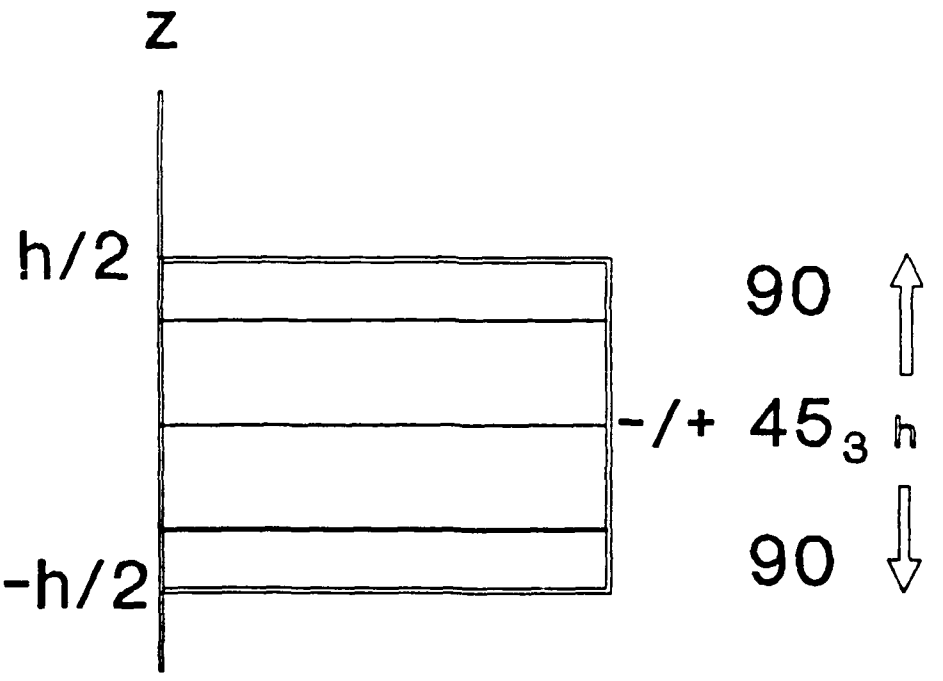

TABLE 5. TRANSFORMED STIFFNESSES - TUBE 1

Ply Angle	Transformed stiffness,GPa	
90	Q11	9.01
-60	Q11	20.08
60	Q11	20.08
90	Q22	138.81
-60	Q22	84.98
60	Q22	84.98
90	Q12	2.70
-60	Q12	24.08
60	Q12	24.08
90	Q66	7.10
-60	Q66	28.48
60	Q66	28.48
90	Q16	0.00
-60	Q16	-15.76
60	Q16	15.76
90	Q26	0.00
-60	Q26	-40.45
60	Q26	40.45

TABLE 6. TRANSFORMED STIFFNESSESS - TUBE 2

Ply Angle	Transformed stiffness,GPa	
90	Q11	9.01
-45	Q11	45.41
45	Q11	45.41
90	Q22	138.81
-45	Q22	45.41
45	Q22	45.41
90	Q12	2.70
-45	Q12	31.20
45	Q12	31.20
90	Q66	7.10
-45	Q66	35.61
45	Q66	35.61
90	Q16	0.00
-45	Q16	-32.45
45	Q16	32.45
90	Q26	0.00
-45	Q26	-32.45
45	Q26	32.45

TABLE 7. $\mathbf{d}^*$ MATRIX - TUBE 1

[d*]

0.11	-0.01	2.36E-18
-0.01	0.01	-6E-18
2.36E-18	-6E-18	0.09

TABLE 8. $\mathbf{d}^*$ MATRIX - TUBE 2

[d*]

0.05	-0.01	1.28E-18
-0.01	0.01	-2.4E-18
1.28E-18	-2.4E-18	0.05

TABLE 9. PREDICTED FREQUENCIES - TUBE 1

MODE	PREDICTED UNDAMPED FREQ (HZ)
1	13.05
2	81.79
3	229.02

TABLE 10. PREDICTED FREQUENCIES - TUBE 2

MODE	PREDICTED UNDAMPED FREQ (HZ)
1	25.56
2	160.20
3	448.61
4	879.03
5	1453.12

TABLE 11. TEST RESULTS - ALUMINUM SPECIMEN

GEOMETRY	l/d	l/b	PREDICTED UNDAMPED FREQ (HZ)	PREDICTED DAMPED FREQ (HZ)	MEASURED FREQ (HZ)	DAMPING RATIO	DELTA %
Rectangle	10	1.20	1304.38	1304.17	915.20	0.013	29.82
I (m^4)	20	2.40	326.10	325.99	249.17	0.018	23.57
1.12E-09	30	3.60	144.93	144.91	120.38	0.011	16.93
A (m^2)	50	6.02	52.18	52.16	49.38	0.019	5.32
0.000335	100	12.05	13.04	13.04	12.93	0.018	0.84
Solid Cylinder	10	10	376.54	376.21	286.68	0.030	23.80
I (m^4)	20	20	94.14	94.04	80.85	0.032	14.03
6.46E-09	30	30	41.84	41.82	37.58	0.021	10.14
A (m^2)	50	50	15.06	15.05	14.20	0.032	5.63
0.000285	70	70	7.68	7.68	7.35	0.029	4.27
Square Shell	10	10	586.87	586.25	472.00	0.032	19.49
I (m^4)	20	20	146.72	146.55	126.13	0.034	13.93
3.56E-09	30	30	65.21	65.16	60.28	0.027	7.49
A (m^2)	50	50	23.47	23.45	22.04	0.035	6.00
0.0000646	90	90	7.25	7.24	6.94	0.030	4.13
Circular Shell	10	10	310.68	310.57	203.51	0.019	34.47
I (m^4)	20	20	77.67	77.64	66.59	0.019	14.23
1.03E-08	25	25	49.71	49.69	43.54	0.021	12.37
A (m^2)	30	30	34.52	34.44	30.88	0.048	10.33
0.0000863	40	40	19.42	19.42	18.33	0.009	5.59
rho, Al (kg/m^3)	2700						
E, Al (GPa)	71						

DELTA % = [1- (MEASURED FREQ/PREDICTED FREQ)]

TABLE 12. **Q, D,** AND **d** MATRICES FOR AL

$$[Q]_{Al} = \begin{bmatrix} \frac{E}{1-\nu^2} & \frac{\nu E}{1-\nu^2} & 0 \\ \frac{\nu E}{1-\nu^2} & \frac{E}{1-\nu^2} & 0 \\ 0 & 0 & \frac{E}{2(1+\nu)} \end{bmatrix}$$

$E = 71$ GPa

$\nu = .25$

$$[Q]_{Al} = \begin{bmatrix} 7.57E+10 & 1.89E+10 & 0 \\ 1.89E+10 & 7.57E+10 & 0 \\ 0 & 0 & 2.84E+10 \end{bmatrix}$$

$$[D]_{Al} = \begin{bmatrix} 4.45 & 1.11 & 0 \\ 1.11 & 4.45 & 0 \\ 0 & 0 & 1.67 \end{bmatrix}$$

$$[d]_{Al} = \begin{bmatrix} 0.24 & -0.06 & 0 \\ -0.06 & 0.24 & 0 \\ 0 & 0 & 0.60 \end{bmatrix}$$

TABLE 13. COMPARISON OF BEAM THEORY AND MODIFIED PLATE THEORY PREDICTED FREQUENCIES - AL

	Circular Shell	Mode 1	
L/D	PREDICTED UNDAMPED FREQ (HZ) BEAM THEORY	PREDICTED UNDAMPED FREQ (HZ) MODIFIED PT	DELTA %
10	310.68	310.55	0.04
20	77.67	77.64	0.04
25	49.71	49.69	0.04
30	34.52	34.51	0.04
40	19.42	19.41	0.04

PT = Plate Theory

DELTA % = [1 - (BEAM THEORY FREQ/MODIFIED PT FREQ)]

TABLE 14. TEST RESULTS - COMPOSITE TUBE 1

MODE	PREDICTED UNDAMPED FREQ (HZ)	PREDICTED DAMPED FREQ (HZ)	MEASURED FREQ (HZ)	DAMPING RATIO	DELTA %
1	13.05	13.03	12.72	0.047	2.42
	13.05	13.03	12.72	0.047	2.42
	l/d = 31	l/b =31			
MODE	PREDICTED UNDAMPED FREQ (HZ)	PREDICTED DAMPED FREQ (HZ)	MEASURED FREQ (HZ)	DAMPING RATIO	DELTA %
2	81.79	81.77	82.02	0.019	-0.31
	81.79	81.77	82.02	0.019	-0.31
	l/d = 31	l/b =31			
MODE	PREDICTED UNDAMPED FREQ (HZ)	PREDICTED DAMPED FREQ (HZ)	MEASURED FREQ (HZ)	DAMPING RATIO	DELTA %
3	229.02	229.00	229.89	0.015	-0.39
	229.02	229.00	229.89	0.015	-0.39
	l/d = 31	l/b =31			

DELTA % = [1- (MEASURED FREQ/PREDICTED FREQ)]

TABLE 15. TEST RESULTS - COMPOSITE TUBE 2

MODE	PREDICTED UNDAMPED FREQ (HZ)	PREDICTED DAMPED FREQ (HZ)	MEASURED FREQ (HZ)	DAMPING RATIO	DELTA %
1	25.56	25.55	20.80	0.033	18.58
	25.56	25.55	20.80	0.033	18.58
	25.56	25.55	20.85	0.033	18.39
	25.56	25.55	20.85	0.033	18.39
	l/d = 25	l/b = 25			
MODE	PREDICTED UNDAMPED FREQ (HZ)	PREDICTED DAMPED FREQ (HZ)	MEASURED FREQ (HZ)	DAMPING RATIO	DELTA %
2	160.20	160.17	129.67	0.020	19.04
	160.20	160.17	129.67	0.020	19.04
	160.20	160.16	129.95	0.021	18.86
	160.20	160.16	129.95	0.021	18.86
	l/d = 25	l/b = 25			
MODE	PREDICTED UNDAMPED FREQ (HZ)	PREDICTED DAMPED FREQ (HZ)	MEASURED FREQ (HZ)	DAMPING RATIO	DELTA %
3	448.61	448.23	367.86	0.041	17.93
	448.61	448.23	367.86	0.041	17.93
	448.61	448.23	367.86	0.041	17.93
	448.61	448.32	369.65	0.036	17.55
	448.61	448.32	369.65	0.036	17.55
	448.61	448.37	368.15	0.033	17.89
	448.61	448.37	368.15	0.033	17.89
	l/d = 25	l/b = 25			

DELTA % = [1- (MEASURED FREQ/PREDICTED FREQ)]

TABLE 16. TEST RESULTS - COMPOSITE TUBE 2

MODE	PREDICTED UNDAMPED FREQ (HZ)	PREDICTED DAMPED FREQ (HZ)	MEASURED FREQ (HZ)	DAMPING RATIO	DELTA %
4	879.03	878.65	783.89	0.029	10.78
	879.03	878.66	783.89	0.029	10.79
	879.03	878.43	784.29	0.037	10.72
	879.03	877.60	698.64	0.057	20.39
	879.03	879.03	684.20	0.002	22.16
	879.03	879.03	727.22	0.002	17.27
	l/d = 25	l/b = 25			

MODE	PREDICTED UNDAMPED FREQ (HZ)	PREDICTED DAMPED FREQ (HZ)	MEASURED FREQ (HZ)	DAMPING RATIO	DELTA %
5	1453.12	1453.02	1187.50	0.012	18.27
	1453.12	1453.02	1187.50	0.012	18.27
	1453.12	1453.02	1187.50	0.012	18.27
	1453.12	1453.02	1190.00	0.012	18.10
	1453.12	1453.02	1190.00	0.012	18.10
	1453.12	1453.02	1194.93	0.012	17.76
	1453.12	1453.02	1194.93	0.012	17.76
	l/d = 25	l/b = 25			

DELTA % = [1- (MEASURED FREQ/PREDICTED FREQ)]

Calibration Certificate

Per ISA-RP37.2

Model No. 309A

Serial No. 2720

PO No. _____ **Customer** _____

Calibration traceable to NIST (NBS) thru Project No. 732/241226-88

ICP™ ACCELEROMETER
with built-in electronics

Calibration procedure is in compliance with MIL-STD-45662A and traceable to NIST (NBS).

CALIBRATION DATA

Voltage Sensitivity	4.96	mV/g
Transverse Sensitivity	3.8	%
Resonant Frequency	120	kHz
Time Constant	0 .1	s
Output Bias Level	12.5	V

KEY SPECIFICATIONS

Range	1000	± g
Resolution	0.02	g
Temp. Range	-40/+150	°F

METRIC CONVERSIONS:
ms $^{-2}$ = 0.102 g
°C = 5/9 x (°F -32)

97

Reference Freq.

Frequency Hz	10	15	30	50	100	300	500	1000	3000	5000	7000	10000
Amplitude Deviation %	-2.8	-2.2	-1.9	-.5	0.0	1.1	1.8	2.5	3.0	4.5	4.2	4.7

FREQUENCY RESPONSE

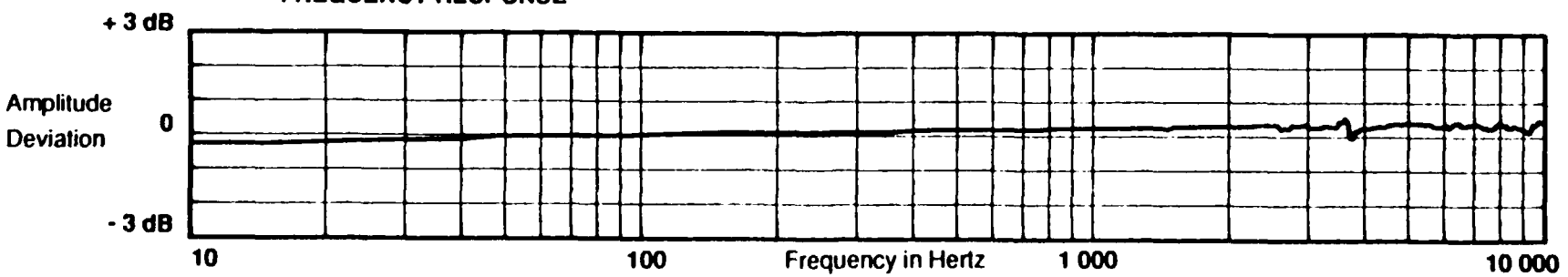

PCB **Piezotronics, Inc.** 3425 Walden Avenue Depew, NY 14043-2495 USA
716-684-0001

Date 5-1-89

Calibrated by _____

Calibration Certificate

Per ISA-RP37.2

Model No. 288A11

Serial No. 391

PO No. _____ Customer _____

Calibration traceable to NIST (NBS) thru Project No. 732/241226-88

ICP™ ACCELEROMETER
with built-in electronics

Calibration procedure is in compliance with MIL-STD-45662A and traceable to NIST (NBS).

CALIBRATION DATA

Voltage Sensitivity	98.9	mV/g
Transverse Sensitivity	4.2	%
Resonant Frequency	32.5	kHz
Time Constant	0 .2	s
Output Bias Level	13.3	V

KEY SPECIFICATIONS

Range	50	± g
Resolution	0.005	g
Temp. Range	-100/+150	°F

METRIC CONVERSIONS:
ms^{-2} = 0.102 g
°C = 5/9 x (°F -32)

86

Reference Freq.

Frequency Hz	10	15	30	50	100	300	500	1000	3000	5000		
Amplitude Deviation %	-1.5	-1.5	-.7	0.0	0.0	-.3	0.0	0.0	0.0	-1.0		

FREQUENCY RESPONSE

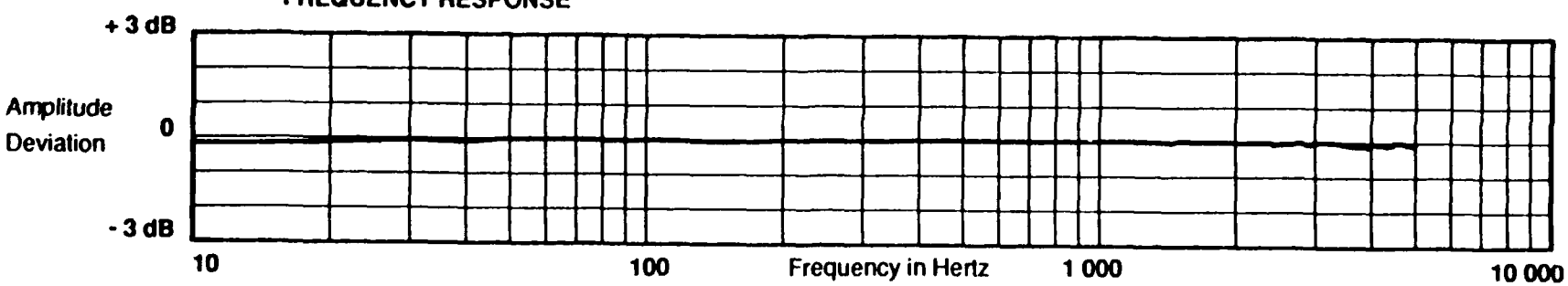

PCB **Piezotronics, Inc.** 3425 Walden Avenue Depew, NY 14043-2495 USA
716-684-0001

Date 4/18/89

Calibrated by P. Jarmuz

ICP CALIBRATION DATA

PCB

Cal Range 0-5 Lbs Input TC >10 sec

Model 288A11 Sens* 1034 mV/ lbs Rise Time 20 µ sec By F. JARMUSZ

S/N 391 Linearity* <1.0 %FS Nat'l Freq 32.5 kHz Date 4-18-89

* By comparison with reference standard per SA S37.10 Zero Based best straight line Output Imp <100 ohms

Calibration of instrumentation used to certify this sensor is traceable to NIST(NBS)
Pcb Piezotronics' calibration procedure is in compliance with MIL-STD-45662

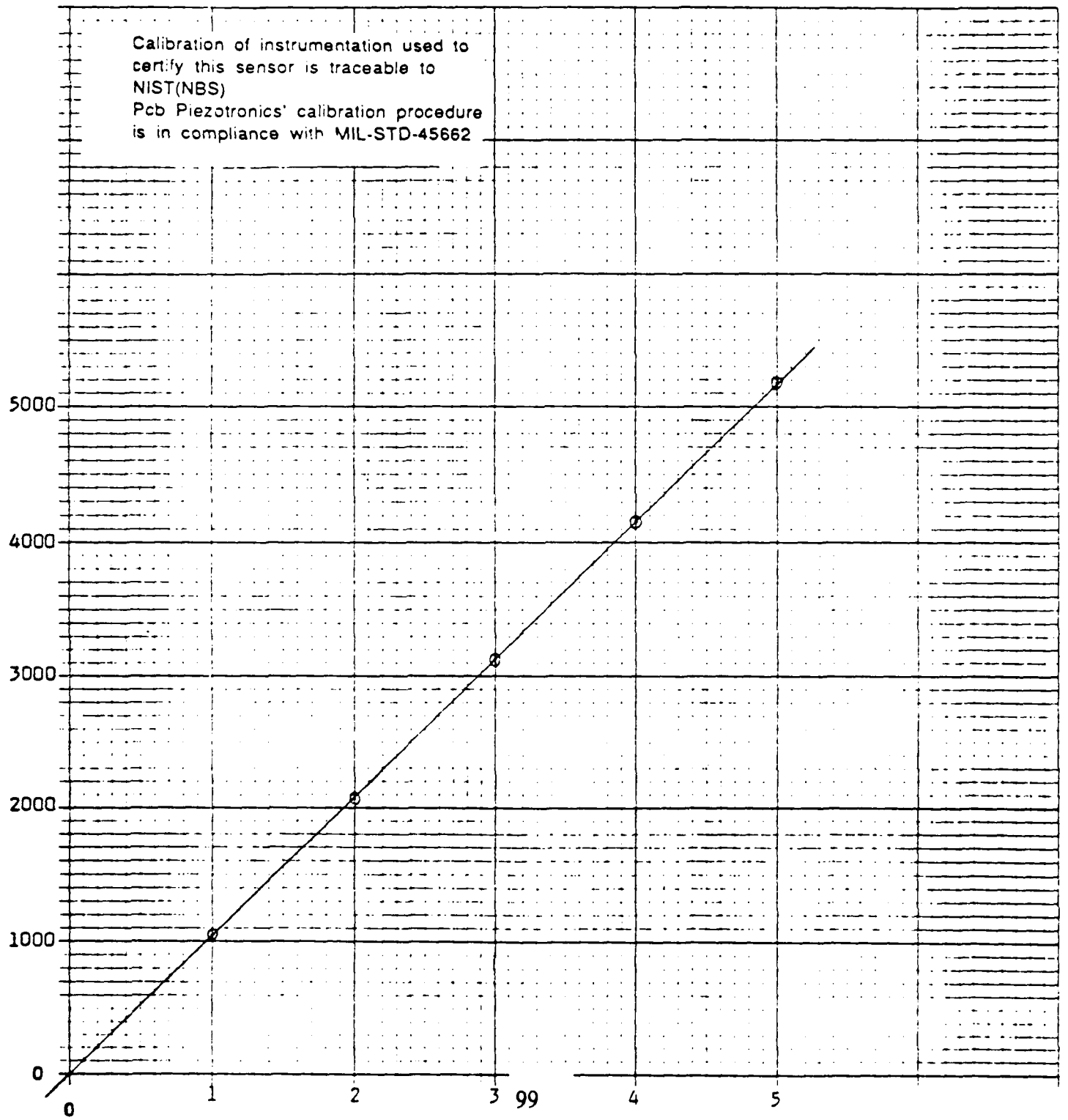

ICP CD787

PCB PIEZOTRONICS, INC.
3425 Walden Avenue Depew NY 14043
Tel 716-684 0001 TWX 710-263 1371

Customer _____

PO Number _____

REFERENCES

1. Dong, S. B., Pister, K. S., and Taylor, R. L., "On the Theory of Laminated Anisotropic Shells and Plates," *Journal of the Aerospace Sciences*,v. 29, pp. 969-975, August, 1962.

2. Dong, S. B., "Free Vibration of Orthotropic Cylindrical Shells," *Acoustical Society of America*,v. 44, pp. 1628-1635, June, 1968.

3. Dong, S. B., and Selna, L. G., "Natural Vibrations of Laminated Orthotropic Shells of Revolution," *Journal of Composite Materials*,v. 4, pp. 2-19, January, 1970.

4. Das, Y. C., "Vibrations of Orthotropic Cylindrical Shells," *Applied Science Research*, v. 12, pp. 317-326, 1964.

5. Das, Y. C., and Rath, B. K., "Vibration of Layered Shells," *Journal of Sound and Vibration*, v. 28, pp. 737-757, 1973.

6. Soedel, W., "Simplified Equations and Solutions for the Vibration of Orthotropic Cylindrical Shells," *Journal of Sound and Vibration*, v. 87, pp. 555-566, 1983.

7. Loewy, R., and Stavsky, Y., "On Vibrations of Heterogeneous Orthotropic Cylindrical Shells," *Journal of Sound and Vibration*, v. 15, pp. 235-256, 1971.

8. Baker, J. K., Bert, C. W., and Egle, D. M., "Free Vibrations of Multilayer Anisotropic Cylindrical Shells," *Journal of Composite Materials*, v. 3, pp. 480-499, July, 1969.

9. Darvizeh, M., and Sharma, C. B., "Natural Frequencies of Laminated Orthotropic Thin Circular Cylinders," *Thin Walled Structures*, v. 2, pp. 207-217, 1984.

10. Weingarten, V. I., "Free Vibrations of Multilayered Cylindrical Shells," *Experimantal Mechanics*, v. 4, pp. 200-205, July, 1964.

11. Bray, F. M., and Egle, D. M., "An Experimental Investigation of the Free Vibration of Thin Cylindrical Shells with Discrete Longitudinal Stiffeners," *Journal of Sound and Vibration*, v. 12, pp. 153-164, 1970.

12. Leissa, A. W., *Vibration of Shells*, U. S. Government Printing Office, Washington D. C., 1973.

13. Meirovitch, L., *Elements of Vibration Analysis*, 2d ed., pp. 205-209, McGraw-Hill Book Co., 1986.

14. Thompson, W. T., *Theory of Vibration with Applications*, 3d ed., pp. 177, Prentice-Hall, 1988.

15. Whitney, J. M., *Structural Analysis of Laminated Anisotropic Plates*, pp. 235-239, Technomic Publishing Co., 1987.

16. Goodier, J. N., and Timoshenko, S., *Theory of Elasticity*, 2d ed., pp. 65-66, McGraw-Hill Book Co., 1951.

17. Tsai, S. W., *Composites Design*, 3d ed., pp. 2.1-2.6, Think Composites, 1986.

18. Jones, R. M., *Mechanics of Composite Materials*, pp. 147-155, Hemisphere Publishing Corp., 1975.

19. Donnell, L. H., *Beams, Plates, and Shells*, pp. 303-442, McGraw-Hill Book Co., 1976.

20. Hahn, H. T., and Tsai, S. W., *Introduction to Composite Materials*, pp. 115-136, 232-239, Technomic Publishing Co., 1980.

21. Newland, D. E., *An Introduction to Random Vibrations and Spectral Analysis*, 2d ed., pp. 113-120, Longman Group LTD, 1984.

22. Ewins, D. J., *Modal Testing: Theory and Practice*, pp. 158-168, Research Studies Press, 1984.

INITIAL DISTRIBUTON LIST

1.	Defense Technical Information Center Cameron Station Alexandria, Virginia 22304-6145	2
2.	Superintendent Attn: Library, Code 1424 Naval Postgraduate School Monterey, California 93943-5000	2
3.	Commandant of the Marine Corps Code TE 06 Headquarters, U. S. Marine Corps Washington, D.C. 20380-0001	1
4.	Prof. Michael R. Gorman Code 31 Naval Postgraduate School Monterey, California 93943-5000	6
5.	Prof. Edward M. Wu Code 31 Naval Postgraduate School Monterey, California 93943-5000	1
6.	Capt Raymond W. Etter 10121 Schoolhouse Woods Ct Burke, Virginia 22015	2
7.	Mr. James L. Koury Composite Materials Lab Air Force Astronautics Laboratory Edwards Air Force Base, California 93523-5000	2
8.	Dr. Alok Das Air Force Astronautics Laboratory Edwards Air Force Base, California 93523-5000	1
9.	Dr. William Scott Code 6063 Naval Air Development Center Warminster, Pennsylvania 18974	1